ESTUDI NUMÈRIC I EXPERIMENTAL DEL SOROLL AERODINÀMIC GENERAT PER UNA TURBINA PETITA D'EIX VERTICAL

Silvana Cecilia Tourn Cremona

UNIVERSITAT ROVIRA i VIRGILI

Characterization of a New Open Jet Wind Tunnel to Optimize and Test Vertical Axis Wind Turbines

SILVANA CECILIA TOURN

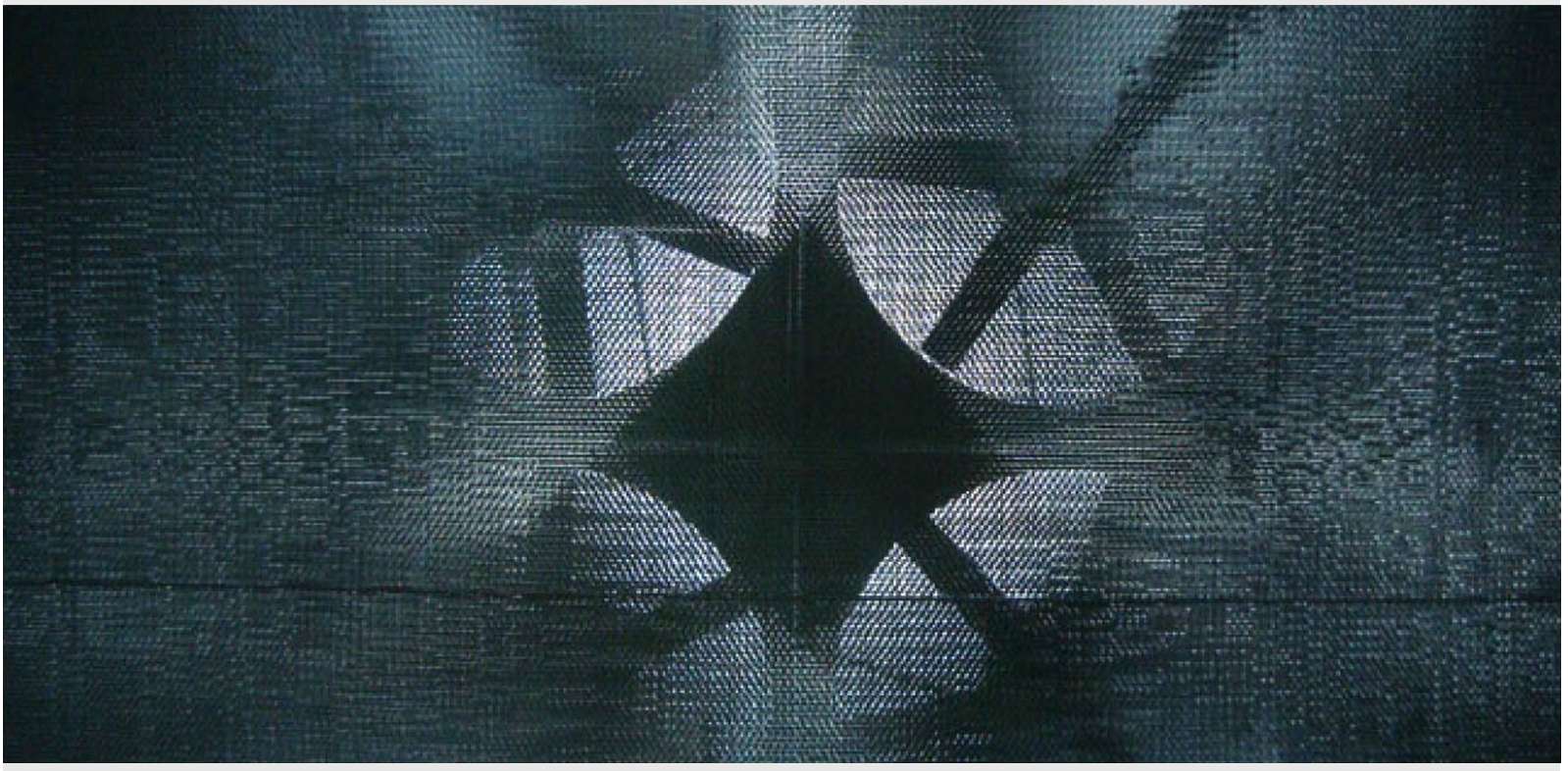

DOCTORAL THESIS
2017

UNIVERSITAT ROVIRA I VIRGILI
ESTUDI NUMÈRIC I EXPERIMENTAL DEL SOROLL AERODINÀMIC GENERAT PER UNA TURBINA PETITA D'EIX VERTICAL
Silvana Cecilia Tourn Cremona

UNIVERSITAT ROVIRA I VIRGILI
ESTUDI NUMÈRIC I EXPERIMENTAL DEL SOROLL AERODINÀMIC GENERAT PER UNA TURBINA PETITA D'EIX VERTICAL
Silvana Cecilia Tourn Cremona

UNIVERSITAT ROVIRA I VIRGILI
ESTUDI NUMÈRIC I EXPERIMENTAL DEL SOROLL AERODINÀMIC GENERAT PER UNA TURBINA PETITA D'EIX VERTICAL
Silvana Cecilia Tourn Cremona

Silvana Cecilia Tourn

Characterization of a New Open Jet Wind Tunnel to Optimize and Test Vertical Axis Wind Turbines

Doctoral Thesis

Supervised by:

Dr. Ildefonso Cuesta Romeo

Dr. Jordi Pallarès Curto

Department of Mechanical Engineering

UNIVERSITAT ROVIRA i VIRGILI

Tarragona, 2017

UNIVERSITAT ROVIRA I VIRGILI
ESTUDI NUMÈRIC I EXPERIMENTAL DEL SOROLL AERODINÀMIC GENERAT PER UNA TURBINA PETITA D'EIX VERTICAL
Silvana Cecilia Tourn Cremona

A mis hijos Leo y Eva, y a su padre Pablo por todo y por tanto.

UNIVERSITAT ROVIRA I VIRGILI
ESTUDI NUMÈRIC I EXPERIMENTAL DEL SOROLL AERODINÀMIC GENERAT PER UNA TURBINA PETITA D'EIX VERTICAL
Silvana Cecilia Tourn Cremona

UNIVERSITAT ROVIRA i VIRGILI

We STATE that the present study, entitled "Characterization of a New Open Jet Wind Tunnel to Optimize and Test Vertical Axis Wind Turbines", presented by Silvana Cecilia Tourn for the award of the degree of Doctor, has been carried out under our supervision at the Department of Mechanical Engineering of this university.

Tarragona, 4 de septiembre de 2017

Dr. Ildefonso Cuesta Romeo

Dr. Jordi Pallarès Curto

UNIVERSITAT ROVIRA I VIRGILI
ESTUDI NUMÈRIC I EXPERIMENTAL DEL SOROLL AERODINÀMIC GENERAT PER UNA TURBINA PETITA D'EIX VERTICAL
Silvana Cecilia Tourn Cremona

Index

Abstract

Urban environmental technologies are the new interest of the society. Based on that, the study of small scale Vertical Axis Wind Turbines (VAWTs) presents motivating challenges. Significant progress in shape, blades design, material and size rotor of the VAWTs over the last few years suggests that these turbines are better than the horizontal axis wind turbines (HAWTs) if placed in urban environment due to their present superior performance in turbulent wind flow.

The available literature presents wind tunnel testing as an alternative solution to expensive online wind power measurements for researchers and small wind turbine developers. The purpose of this endeavor is to present the characteristics and potentials of an Open Jet Wind Tunnel built in our laboratories to support the study of the urban VAWTs.

The design criteria of the new facility were based in the concepts present in the available literature. It is supported by numerical simulation of the geometry designed. The elements of the 4-Winds Open Jet Wind Tunnel are (in the direction of the flow): fans, plenum, flow straighteners and conditioning elements, a contraction and test section. The flow is impelled by four fans of 7.5 kW each, with a diameter of 1 m and placed in a 2.24 m x 2.24 m matrix. Every element is described and analyzed in detail along this research work.

The tunnel has an open test section of 1.5 x 1.5 m^2. It can be operated with exit velocities from 3 m/s to 17 m/s. The characterization of the flow has been carried out with calibrated pitot tubes, cup anemometer and hot wire anemometry. Two different configurations of the test area with and without a ceiling are considered in order to improve the uniformity of the flow in the test section area. The test area with ceiling presents a velocity increase of about 0.5 m/s and an overall reduction of the turbulence intensity of about 3% with respect to the case without the false ceiling. Measurements in the range of available exit velocities show that the cross section, where the velocity and turbulence intensities show an acceptable level of uniformity, has an area of 0.8 x 0.8 m^2 and a streamwise dimension of 2 m from the nozzle exit of the tunnel with ceiling. Non-uniformity of velocity and the turbulence intensity are 5 % and 1% respectively, at

1 m downwind of the tunnel exit at tunnel speeds between 5 m/s and 15 m/s. These characteristics are similar as those in an open jet wind tunnel installed at Delft University of Technology of the Netherlands built with same purpose.

The analysis of the velocity signals indicates that the spectra follow a "normal Atmospheric Boundary Layer (ABL) turbulence" behaviour with a production range of around $f/U \approx 10$ (where f is the frequency and U is the mean velocity) followed by an inertial subrange shown by a -2/3 slope turbulence. Davenport spectrum represented reflects the tunnel spectrum quite well.

Studies with a cup anemometer calibrated were also carried out. First, the blockage effect study of the cup anemometer on pitot tubes were made in order to define the optimal position of the measuring instruments. Second, measurements of the mean velocities without and with false ceiling at different positions from de nozzle (x-axis), with 4 pitot tubes + cup anemometer, then with cup anemometer only positioned in the centre of the test area and finally with 4 pitot tubes only was carried out. Finally, the calibration results of the cup anemometer with the false ceiling are explained. The results of the first study show less influence between pitot tubes and cup anemometer at 30 cm of distance from each other. With the false ceiling, the values of the flow velocities measured by de pitot tubes and anemometers are more coincident. In the cup anemometer calibration, the best linear fit of the anemometer response was found when the cup anemometer was positioned at x = 1 m from the nozzle exit (x-axis).

Resumen

Las tecnologías ambientales urbanas son el nuevo interés de la sociedad. Basado en esto, el estudio de las turbinas eólicas de eje vertical (VAWTs) presenta desafíos motivadores. Avances significativos en la forma, el diseño de las palas, el material y el tamaño del rotor de las VAWTs en los últimos años, sugieren que estas turbinas son más adecuadas para entornos urbanos que las turbinas de viento de eje horizontal (HAWTs), debido a que presentan un rendimiento superior en flujos de viento turbulentos.

La literatura disponible demuestra que el túnel de viento es una solución alternativa a las costosas mediciones directas de energía eólica para los investigadores y desarrolladores de pequeñas turbinas de viento. El propósito de este trabajo es dar a conocer las características y potencialidades de un túnel de viento de chorro libre construido en nuestros laboratorios para apoyar el estudio de los VAWTs urbanas.

El criterio de diseño de la nueva instalación se basa en conceptos presentes en la literatura disponible. Este criterio es reforzado con la simulación numérica de la geometría diseñada.

Los elementos del túnel de viento de sección de prueba abierta 4-Winds son (en la dirección del flujo): ventiladores, cámaras de tranquilización, rectificadores y elementos de acondicionamiento de flujo, una contracción y la sección de pruebas.

El flujo es impulsado por cuatro ventiladores de 7,5 kW cada uno, con un diámetro de 1m y colocados en una matriz de 2.24 m x 2.24 m. Cada elemento se describe y analiza en detalle a lo largo de este trabajo de investigación.

El túnel tiene una sección de prueba abierta de 1.5 x 1.5 m^2. Puede operar a velocidades de salida de 3 m/s a 17 m/s. La caracterización del flujo se ha realizado con tubos de pitot calibrados, anemómetro de cazoletas y anemometría de hilo caliente. Se consideran dos configuraciones diferentes de la zona de ensayo, con y sin techo. La sección de prueba con techo presenta un incremento de velocidad de aproximadamente 0,5 m/s y una reducción global de la intensidad de turbulencia de aproximadamente 3% con respecto al caso sin el falso techo.

Las mediciones en el rango de velocidades de salida disponibles muestran que la sección transversal, donde las velocidades e intensidades de turbulencia muestran un nivel aceptable

de uniformidad, tiene una superficie de 0,8 x 0,8 m^2 y una dimensión en sentido de la corriente de flujo de 2 m de la salida de la boquilla del túnel. La velocidad no uniforme y la intensidad de la turbulencia son de 5% y 1%, respectivamente, a 1 m de la salida del túnel a una velocidad del túnel entre 5 m/s y 15 m/s. Estas características son similares a un túnel de viento de sección de prueba abierta instalado en la Universidad de Tecnología de Delft construido con el mismo propósito.

El análisis de las señales de velocidades indica que el espectro sigue el comportamiento de la "turbulencia de capa límite atmosférica normal (ABL)" y que se produce en un rango alrededor de $f/U \approx 10$ (siendo f la frecuencia y U la velocidad media) seguido de una sub rango inercial que muestra una pendiente negativa de turbulencia de - 2/3. El espectro de Davenport representado refleja bastante bien el espectro del túnel.

También se realizaron estudios con un anemómetro de cazoletas calibrado. En primer lugar, se realizó el estudio del efecto de bloqueo del anemómetro de cazoletas sobre los tubos de pitot, a fin de definir la posición óptima de los instrumentos de medida. En segundo lugar, se llevaron a cabo mediciones de las velocidades medias sin y con falso techo, a diferentes posiciones de la salida (eje x), con 4 tubos de pitot + el anemómetro de cazoletas, luego sólo con el anemómetro de cazoletas colocándolo en el centro del área de ensayo, y finalmente sólo con 4 tubos de pitot. Para concluir, se explican los resultados de calibración del anemómetro de cazoletas con falso techo. Los resultados del primer estudio muestran menos influencia entre los tubos de pitot y el anemómetro de copa a partir de 30 cm de distancias entre sí. La gráfica de los segundos estudios presenta una mejor distribución del flujo con el falso techo, es decir, los valores de las velocidades de flujo son más coincidentes. En la calibración del anemómetro de cazoletas, se encontró el mejor ajuste lineal a la respuesta del anemómetro cuando se lo colocó a x = 1 m de la salida de la contracción (en el eje x).

Publications and Conferences

Publication in Journal Papers

S. Tourn, J. Pallarès, I. Cuesta and U. S. Paulsen, "Characterization of a New Open Jet Wind Tunnel to Optimize and Test Vertical Axis Wind Turbines", Journal of Renewable and Sustainable Energy **9**, 033302 (2017); doi: http://dx.doi.org/10.1063/1.4982750 (Received 12 June 2016; accepted 17 April 2017; published online 2 May 2017).

Contribution to Conferences

S. Tourn, R. Gilabert, V. Sánchez, J. Pallarès, A. Vernet, I. Cuesta and U.S. Paulsen. "Characterization of a New Open Jet Wind Tunnel to Optimize and Test Vertical Axis Wind Turbines using Flow Visualization and Measures". The European Wind Energy Association (EWEA). March 2014. Poster presentation. Barcelona, Spain.

UNIVERSITAT ROVIRA I VIRGILI
ESTUDI NUMÈRIC I EXPERIMENTAL DEL SOROLL AERODINÀMIC GENERAT PER UNA TURBINA PETITA D'EIX VERTICAL
Silvana Cecilia Tourn Cremona

Internship

Institution: Wind Energy Department, Risø Campus, Technical University of Denmark.

Advisor: Uwe Schmidt Paulsen

Dates: October to December 2012

Objective: Improvement of flow and turbulence analysis of the open jet wind tunnel and design of a small Vetical Axis Wind Turbine including scaling laws for wind tunnel models.

UNIVERSITAT ROVIRA I VIRGILI
ESTUDI NUMÈRIC I EXPERIMENTAL DEL SOROLL AERODINÀMIC GENERAT PER UNA TURBINA PETITA D'EIX VERTICAL
Silvana Cecilia Tourn Cremona

Agradecimientos

El trabajo presentado en esta memoria ha sido desarrollado dentro del grupo de investigación Experiments, Computation and Modelization in Fluid Mechanics and Turbulence (ECoMMFiT) adscrito al Departamento de Ingeniería Mecánica de la Escola Tècnica Superior d'Enginyeria Química (ETSEQ) de la Universitat Rovira i Virgili bajo la dirección conjunta de los Drs. Jordi Pallarès e Ildefonso Cuesta.

Quisiera agradecer:

A mis directores Jordi e Ildefonso, sin ellos esta tesis no hubiera sido posible. Gracias por su gran ayuda y por tanta paciencia.

Al Dr. Robert Gilabert, gracias por su guía durante los ensayos y análisis de medidas, por la bibliografía prestada y por otorgarme su valioso tiempo.

Al Dr. Anton Vernet por brindarme sus conocimientos cuando los necesité y a Valentín Sánchez por su valorable asistencia en la puesta a punto del túnel.

Al Dr. Uwe Schmidt Paulsen por su guía durante la estancia en DTU Wind Energy Risø Campus, en Roskilde, Dinamarca. Many thanks to give me the opportunity to know the wind energy world. Also for your kind of help and your friendship.

A todos mis compañeros del ECoMMFiT, a los que siguen en él y a los que ya se fueron. De todos me he quedado con los mejores recuerdos.

A mis amigos David Martínez y Lindsay Ryan Valerio, por los cafés, por su apoyo e invalorable amistad a lo largo de toda mi estancia en Tarragona. Los extraño tanto.

A mi adorable Marie (compartir piso contigo fue para construir una bonita amistad).

A mis amigas, las hermanas Liva, que han cuidado de Leo con tanto amor desde que he regresado a Argentina, para hacer realidad este documento escrito.

A mi familia, en especial a mi mamá por su apoyo y amor incondicional de siempre.

A mi compañero Pablo, quien me siguió en la aventura del doctorado y quien me apoya cada día para hacer de esto un hecho. Gracias por confiar en mí y construir conmigo una familia. Te amo.

Finalmente agradecer el soporte financiero concebido por el Ministerio de Economía y Competitividad Español en virtud de la beca otorgada CTQ2013-46799-C2-1-P.

Nada más me queda por agradecer a los miembros del tribunal por aceptar juzgar esta tesis doctoral y a todas las personas que, directa o indirectamente, han participado en su elaboración.

List of Tables

UNIVERSITAT ROVIRA I VIRGILI
ESTUDI NUMÈRIC I EXPERIMENTAL DEL SOROLL AERODINÀMIC GENERAT PER UNA TURBINA PETITA D'EIX VERTICAL
Silvana Cecilia Tourn Cremona

List of Figures

UNIVERSITAT ROVIRA I VIRGILI
ESTUDI NUMÈRIC I EXPERIMENTAL DEL SOROLL AERODINÀMIC GENERAT PER UNA TURBINA PETITA D'EIX VERTICAL
Silvana Cecilia Tourn Cremona

Chapter 1

INTRODUTION

The increasing demand for clean and affordable energy all over the world will without doubt lead to an increasing demand for small wind industries.

Nowadays, urban environmental technologies are a very attractive alternative. Based on that, the study of small scale Vertical Axis Wind Turbines (VAWTs) presents motivating challenges due to the fact that these turbines are better than the horizontal axis wind turbines (HAWTs) if placed in urban environment because of their present superior performance in skewed flow [1].

The concept of urban wind turbines is quite new and technology is not yet fully developed. The publication about energy in Spain entitled "El libro de la Energía en España 2013" [2] reports that energy consumption in Spain has been evolving in towards a more diversified and balanced structure, with a higher participation of renewable energy sources. Then this book mentions the *Centro de Investigaciones Energéticas, Medioambientales y Tecnológicas* (CIEMAT) as a world reference centre specializing in medium and small power wind turbines thanks to the accreditation of the National Entity of Accreditation (ENAC) and according to UNE-EN ISO/IEC 17025:2005 for the performance of power curve tests (IEC 61400-12-1 standard), duration (IEC 61400-2 standard), noise emission (IEC 61400-11 standard) and operation and safety (IEC 61400-2 Standard). The CIEMAT together with the Centre for Renewable Energy Development (CEDER) has been developing and validating a simulation model in computational fluid dynamics (CFD) of the wind conditions in urban environment and its influence on the behaviour of the small wind turbines installed in the cover of the research building in CEDER. Given the growing international interest in improving energy management in buildings, these technologies are presented as a suitable alternative.

Figure 1 shows an example of small vertical axis wind turbine mounted in an urban area. Technically, there are several definitions of small wind turbines: The most important international standardization body, the International Electrotechnical Commission (IEC), defines Small Wind Turbines (SWTs) in standard IEC 61400-2 as having a rotor swept area of less than 200 m^2, equating to a rated power of approximately 50 kW generating an under 1.000 V AC or 1.500 V DC. In addition to this standard, several countries have set up their own definition of small wind turbines. The discrepancy of the upper capacity limit of small wind ranges between 15 kW to 100 kW for the five largest small wind countries (Canada, China, Germany, UK and USA). The major pattern of today`s upper limit capacity leans towards 100 kW. This is largely caused by the leading role of the North American and European market [3].

Figure 1: A small Quiet revolution QR5 Gorlov type vertical axis wind turbine in Bristol, England.

With these technologies in mind, a new research line was opened in the ECoMMFiT[1] research group in Tarragona (Spain). The available literature presents wind tunnel testing as an alternative solution to expensive online wind power measurements for researchers and small wind turbine developers. The purpose of this endeavor is to present the

[1]ECoMMFiT: Experimentation, Computation and Modelization in Fluid Mechanics and Turbulence (http://ecommfit.urv.es).

characteristics and potentials of an open jet wind tunnel built in our laboratories to support the study of the urban VAWTs.

Chapter 1 presents a literature review of wind tunnel facilities and a list of other existing open jet wind tunnels. Then, the technical objectives and approach are described and an outline of this thesis is provided.

1.1 Literature review and comparison with existing wind tunnels

The literature presents different concepts to design Open Jet Wind Tunnels (OJWTs). Some of them have a closed-circuit design with a closed or semi-closed test section, from which the air flow exiting the nozzle enters the collector [4, 5].

The others are open circuit tunnels [6, 7, 8, 9] where the open jet from the nozzle is not collected, but expands freely into a larger room. The major test capabilities of these wind tunnels are aerodynamic testing and aeroacoustic testing.

Compared to traditional wind tunnel testing, an open jet wind generating facility offers more capabilities and features for testing wind turbine [10]. This configuration allows the use of higher blockage ratios, it provides excellent access to the model and it facilitates flow field measurements [11]. Studies of wind turbines using OJWTs are presented in the available literature.

Some of them include analysis of the wake because it is the driving phenomenon for energy recovery in a wind farm and for the interaction between wind turbines [12]. Others investigate the aerodynamic performances of blades of a small-scale VAWT in order to improve the low blade speed ratios [13]. Symmetrical blades are usually implemented a thick NACA 0020 profile was used in this manuscript. The effects of various parameters on the power production of a small wind turbine, such as the jet diameter, the distance of the wind turbine from the jet nozzle and the wind turbine hub diameter, are investigated [10]. This paper considered a small wind turbine with a hub radius of r_0=0.1R and c_p= 0.4 (where R is the jet radius and c_p is the power coefficient). Finally, the measurements of an H-Darrieus in the skewed flow on a roof [14] are available.

In most of the turbulent jets studied theoretically or experimentally, the wind speed is always assumed uniform and constant at the outlet of the nozzle. In OJWTs a uniform flow could be achieved just at the exit of the nozzle, i.e. in the potential core. Reference [12] presents a detailed measurement and analysis of the vortical structures in the wake of a horizontal axis wind turbine (rotor diameter of 0.6 m). The studies had been carried out in the open-jet wind-tunnel of the Delft University of Technology (TU Delft) applying Stereoscopic Particle Image Velocimetry (SPIV), in order to visualize the dependency between the wake re-energizing process and the tip-vortex helix development, in the near and far wake of the turbine. The OJWT of TU Delft facility has an outlet diameter of 3 m that is placed in a large room with a width of 13 m and a height of 8 m. It can handle very large models that obstruct airflow quite considerably.

Reference [13] employed Zero-Net Mass Flux (ZNMF) actuation on an H-type VAWT blade. The ZNMF actuation [15] and [16] is an alternative flow control technique that has been traditionally employed to delay static stall and mitigate flow separation on aircraft wings. As its name suggests, there is no net transfer of mass, but enhances surrounding flow through a non-zero transfer of momentum. This can be achieved using an oscillating piston or diaphragm operating within an enclosed cavity through an orifice. Additionally, this arrangement avoids the need for fluid reservoirs and complex plumbing necessary for steady blowing or suction. This study, therefore, suggests that reduced oscillatory loads and more robust output power can be achieved with zero-net mass flux actuation on VAWT operating at low blade-speed ratios. Consequently, the findings have positive practical implications for the design of small-scale VAWT for widespread use in the urban environment.

Reference [11] exposes a literature review of wind generating facilities for testing wind turbines. It lists various studies performed and it highlights the capabilities and features of the OJWTs over other designs of wind tunnels to study wind turbines. In this work the structure of circular open jet flows is reviewed and the effects of various parameters on the power production of a small wind turbine are investigated and the results are addressed as well.

Reference [14] is a doctoral thesis. That deals with wind energy conversion in the built environment. It gives a description of the wind resources in the built environment that can be converted into energy by a wind turbine. This work implements mathematical, experimental and computational fluid dynamic tools. The experimental measurements of this thesis were carried out in the open jet wind tunnel of Delft University of Technology. The open jet wind tunnel is made of a large circular tube that encloses a fan at the suction side of the tube. There is no collector for the flow and the hall is used as return channel for the flow.

Based in all of these studies an open jet wind generating facility was decided to be designed.

Then a review of existing wind tunnels in Spain was conducted. The aerodynamic testing facilities of the University Institute of Microgravity "Ignacio Da Riva" of the Technical University of Madrid (IDR/UPM) constitute a reference center for Spanish industry. Every wind tunnel of IDR/UPM has been developed and built with human and technical resources from the institute. Visiting all testing facilities of the Institute, the S4 wind tunnel was found similar to our model. The S4 wind tunnel is a closed chamber wind tunnel with an open-circuit. However, it can be used as an open chamber wind tunnel with collector. Also two slightly larger replicas of this wind tunnel have been built (S4/2 and S4/3) at Montegancedo campus to increase the capacity of the calibration laboratory. They are designed to fulfill the specific requirements of industrial anemometer calibration in accordance with the Measuring Network of Wind Energy Institutes called MEASNET.

The 4-Winds OJWT has a similar purpose and similar characteristics as the open jet wind tunnel installed at Delft University of Technology reported by Mertens [14]. It can be seen that the 4-Winds OJWT is smaller and it produces flow uniformities and turbulence intensities similar to those of the tunnel at Delft.

The characteristics of various existing open jet wind tunnels are summarized in Table 1. The facilities shown in the table are used for research on wind turbines, aviation industries, and anemometry calibrations. Some of them include anechoic test sections for acoustic measurements and can generate high flow speeds and very low turbulence levels.

Facility	**OJWT[a] TU Delft**	**4W-OJWT Tarragona**	**S4 WT IDR/UPM[b]**	**OJ UNSW[c]**	**SWT[d] Virginia Tech**
Country	Netherlands	Spain	Spain	Australia	U.S.
Cross section	Circular	Square	Square	Circular	Square
Test Section Size (m)	2.24 diam.	1.5 x 1.5	0.9 x 0.9	0.76 diam.	1.83 x 1.83
Test SectionType	Open	Open	Closed/Open[e]	Open	Closed/Open[e]
Tunnel length (m)	10.85	4	12	-	-
Maximum tunnel speed (m/s)	14	17	26	20	80
Non-uniformity of velocity (%)	7[f]	5[g]	-	-	-
Turbulence level (%)	0.8[f]	1[h]	0.2	0.2	0.01 - 0.03[i]

Table 1: Main characteristics of the open jet wind tunnels analyzed.

[a]OJWT TU Delft: Open Jet Wind Tunnel, the Delft University of Technology [14].
[b]S4 WT IDR/UPM: S4 Wind Tunnel, Instituto Universitario de Microgravedad Ignacio Da Riva/Universidad Politécnica de Madrid [17, 18].
[c]OJ UNSW: Open Jet, the University of New South Wales [19].
[d]SWT: Stability Wind Tunnel, Virginia Tech. [4].
[e]Closed/Open: The tunnel has a removable test section, i.e., it can be used as a closed test section or an open test section.
[f]At a test section of 0.9 x 1.2 m^2, 1.2m downwind of the tunnel exit with a tunnel speed of 6 m/s.
[g]At a test section of 0.8 x 0.8 m^2, 1m downwind of the tunnel exit at tunnel speeds between 5 m/s and 15 m/s (see Figure 34).
[h]Maximum value at a test section of 0.8 x 0.8 m^2, 1m downwind of the tunnel exit at tunnel speeds between 5 m/s and 15 m/s (see Figure 36).
[i]Turbulence levels are 0.016% at 12 m/s and increase gradually with flow speed to 0.031% at 57 m/s [4].

1.2 Objectives

The ECoMMFiT research group integrates experimental, computational and analytical tools to advance in the knowledge of the structure of flows and their effect on the heat and mass transfer processes. So far, the research group had not ventured studying wind turbines. With the desire to contribute in this area and encouraged by the growing interest in urban wind turbines use, the experimental study of wind turbines was proposed.

To perform the experimental study, the available literature sources present the wind tunnel as an essential experimental tool. The wind tunnels play an important role in both teaching and experimental scientific research for a vast range of subjects in aerodynamics. It is often a rapid and accurate tool to conduct aerodynamic research, to support design decisions and to validate numerical methods.

Based on that, the thesis goal is to design and build an Open Jet Wind Tunnel facility at the Universitat Rovira i Virgili. A tunnel design methodology has to be developed to optimize the design of the wind tunnel circuit to meet these constraints within the allotted space and budget. The modern computational tools available in the research group will be used to facilitate and validate the design of wind tunnel components. The wind tunnel has to be fabricated and then characterized by carrying out aerodynamic measurements.

1.3 Technical Approach

a) Design a new open jet wind tunnel to develop studies of small wind turbines.
b) Validate the design using CFD.
c) Select and acquire different components of the wind tunnel (fans, fan inverter, screens, honeycomb, and construction materials).
d) Fabricate the wind tunnel components.
e) Select, acquire and assemble measuring instruments for characterization.
f) Characterize the open jet wind tunnel by making aerodynamic measurements that include:

- Flow uniformity measurements.
- Turbulence intensity measurements.
- Cup anemometer calibration.

1.4 Thesis Organization

The remaining chapters of this thesis are organized as follows. Chapter 2 describes the design procedure adopted for the wind tunnel components, finishing with a computational analysis performed to predict the flow quality of the open jet design. Chapter 3 discusses the fabrication of the wind tunnel facility. Chapter 4 deals with the setup and procedure for the experiments undertaken to characterize the facility. Chapter 5 describes the experimental results and discussions concerning the facility characterization. Chapter 6 provides summary, key conclusions, and offers suggestions for future work.

UNIVERSITAT ROVIRA I VIRGILI
ESTUDI NUMÈRIC I EXPERIMENTAL DEL SOROLL AERODINÀMIC GENERAT PER UNA TURBINA PETITA D'EIX VERTICAL
Silvana Cecilia Tourn Cremona

Chapter 2

DESIGN OF THE 4-WINDS OPEN JET WIND TUNNEL

This chapter deals with the details of the aerodynamic design of the wind tunnel components. It begins with the design criteria and continues with the aerodynamic considerations to estimate the power of the driving fan. A brief discussion about the computational analysis made to predict the flow quality of the wind tunnel is also provided.

2.1 Design Criteria

The present wind tunnel was designed with urban VAWTs dimensions in mind. The validity of the tests in a tunnel with a scale model requires the existence of geometric, kinematic and dynamic similarity between the flow around the model and the flow around the obstacle under atmospheric conditions. This means that the model should be a replica of the real turbine and should also present certain dimensionless parameters equal in both flows, i.e. between the flow under real atmospheric conditions and the flow generated in the wind tunnel. A central issue in the sizing of a low speed wind tunnel is the achievable Reynolds number for the model that can be accommodated. The Reynolds number is defined as the ratio of momentum forces to viscous forces expressed in terms of geometrical parameters of the obstacle (the characteristic length L) and the flow (density ρ, speed, υ, and dynamic viscosity, μ).

$$\mathrm{Re} = \frac{inertial\_forces}{vicous\_forces} = \frac{\rho \upsilon L}{\mu} \qquad (1)$$

In the design of a low-speed wind tunnel, the Mach number results to be an irrelevant parameter. However, it should be built with the higher as possible Reynolds number. Increasing the value of this parameter means increasing the value of the velocity in the test chamber, υ, augmenting the value of the characteristic length test models, L, or both. The value of L is limited by the front cross-sectional area of the test chamber, and then the model cannot excessively block the duct. A typical maximum value of the solid blockage can be 0.1, meaning that the test chamber should have a section with an area at least an

order of magnitude higher than L^2. The solid blockage is often computed as the ratio of the frontal area of the object and the cross section of the wind tunnel [1], and it is usually expressed in percentage. So, the power required is proportional to L^2v^3, so it is more advantageous to increase the value of the Reynolds number by making the size of the test chamber larger. This criterion is reinforced when one considers that, due to the low speed; the aerodynamic loads on the various parts of the tunnel will also be low allowing a cheaper construction.

Accordingly, the Reynolds number was defined once the test section size and the maximum wind speed were established. The maximum wind speed for the present wind tunnel was set to be about 20 m/s for a nozzle hydraulic diameter of 1.5 m. Another design criterion is the quality of the flow in the test section, which depends on the turbulence intensity. This parameter is less strict in tunnels for non-aeronautical testing [20]. As a design goal, a value of 5% in the uniform section was defined. The available building space for the facility was 12 m in length, 5 m in width and 4 m in height.

2.2 Wind tunnel layout

Based on the literature review, the concept of the open jet wind tunnel without collector has the advantage of lower cost and less required space. According to this and after a computational study, it was decided to design the wind tunnel as an open-circuit tunnel with components and dimensions shown in **Figure 2**.

The tunnel, named "4-Winds", is an open jet type tunnel, powered by 4 fans with an open test section and open circuit. The elements of this wind tunnel are (in the direction of the flow): fans, plenum, flow straighteners and conditioning elements, a contraction and test section respectively. The flow is impelled by four fans of 7.5 kW each, with a diameter of 1 m and placed in a 2.24 m x 2.24 m matrix. The fans feed 1m long plenum chambers with a safety screen at the end. A honeycomb and two grids are placed windward to reduce flow turbulence intensity and increase speed uniformity. All these elements complete the settling chamber of the new facility. They can be easily removed for maintenance. Finally, the open jet exits into the test section from the contractor nozzle. The contraction with a ratio of 2.23 and a length of 1 m increases the flow speed.

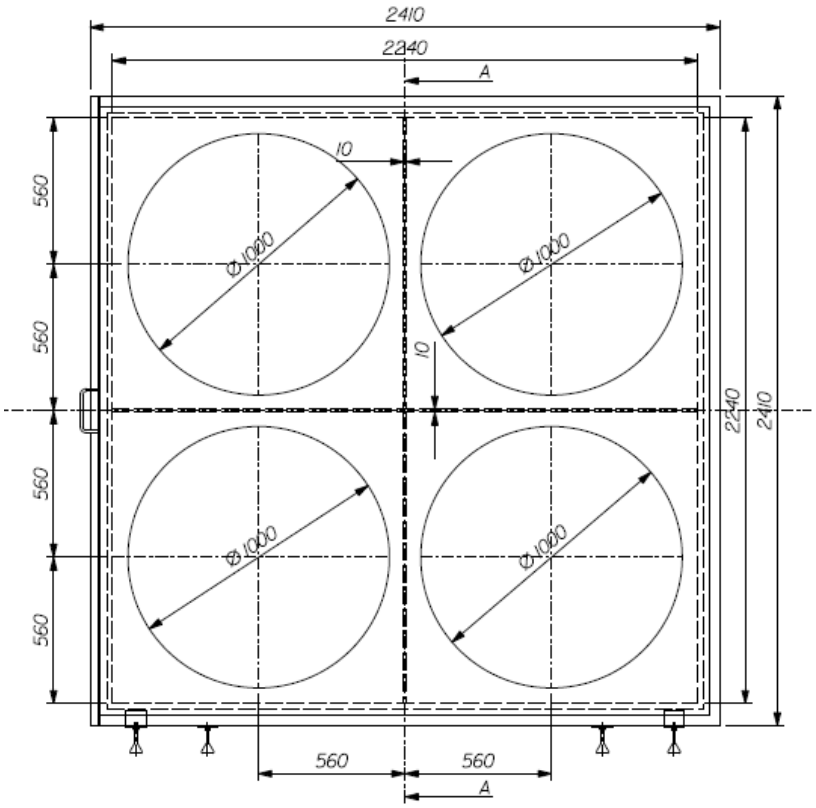

2.a. Back view

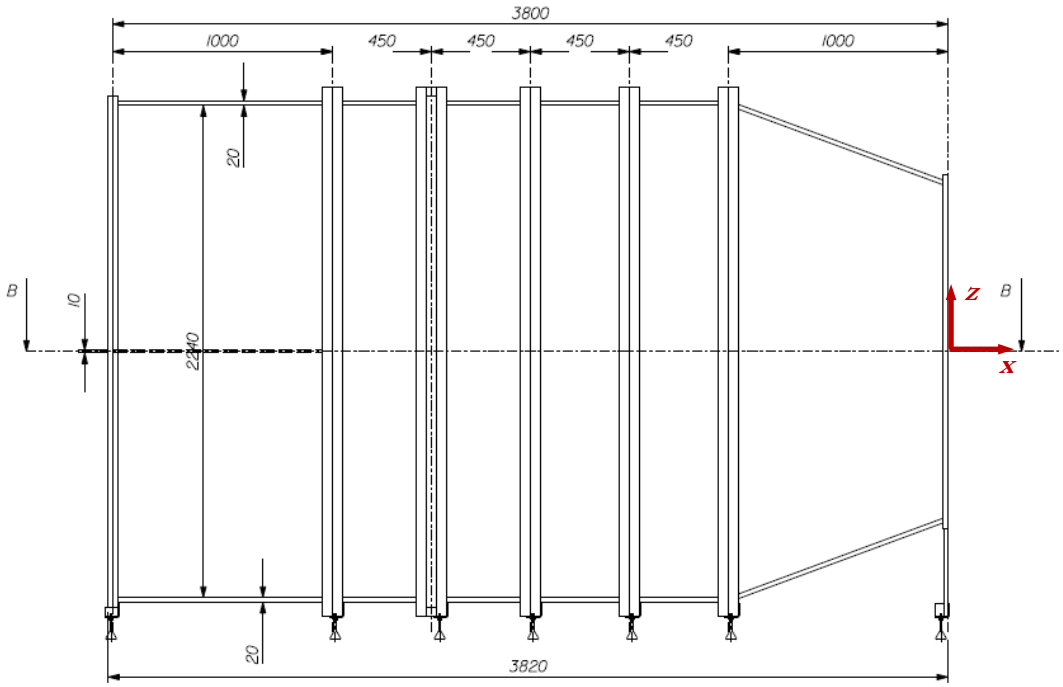

2.b. Side view

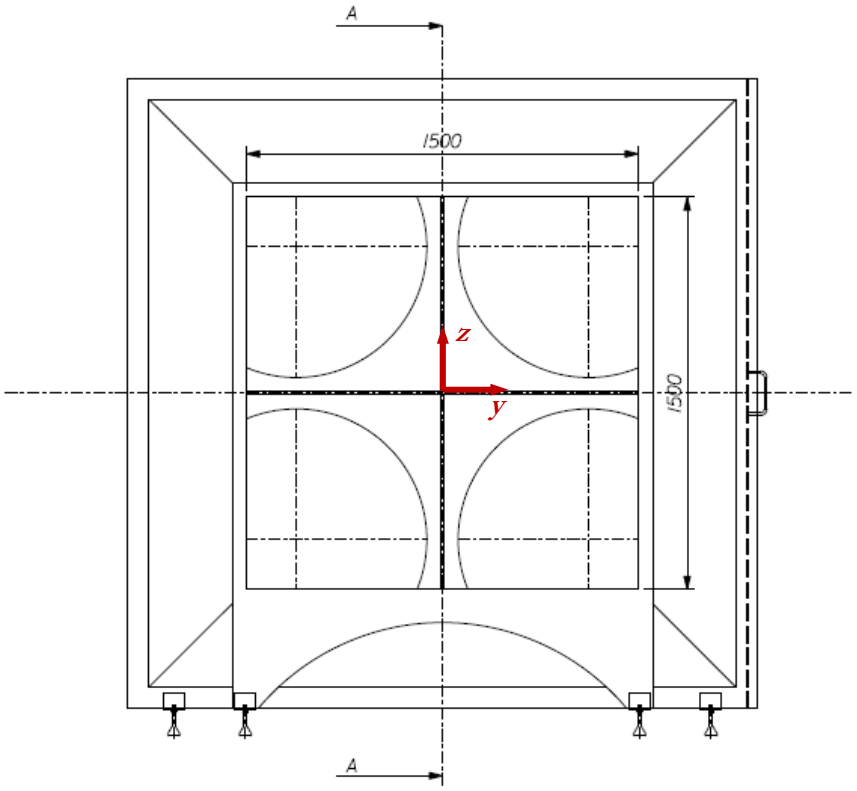

2.c. Front view

2.3. Aerodynamic Design

The aerodynamic considerations were established once the general layout was defined. The size of the nozzle exit is based on the solid blockage effect and this defines the dimensions of the other wind tunnel components. Solid blockage is often addressed as a function of frontal area of the object and the wind tunnel's cross section, and is often expressed in percentage. Taking into account the frontal swept area of a small urban VAWT, i.e. around 0.5 m x 0.5 m, a nozzle exit cross section (1.5 m x 1.5 m) was defined and resulted in a blockage ratio of around 11%.

The 4-Winds OJWT has a square-to-square contraction and square cone shape. A jet with a maximum speed of approximately 20 m/s in the test section was proposed. The power of the driving fan was estimated bearing in mind the above mentioned maximum speed and the summation of pressure losses in the wind tunnel.

Friction losses are due to fluid viscosity and occur along the length of the duct, and they are calculated by the Darcy-Weisbach's equation.

$$\Delta P_f = f \cdot \left(\frac{L}{D_H} \right) \cdot \left(\frac{\rho . v^2}{2} \right) \qquad (2)$$

Where ΔP_f is the friction losses in terms of total pressure; f friction coefficient; L length of the duct; D_H hydraulic diameter; g gravity velocity and v mean speed of flow. As a first calculation with a big hydraulic diameter in mind, considering a low roughness material and considering the Reynolds number in the cross-constant area pipe, a friction coefficient of 0.02 (using Moody diagram) was acquired.

Dynamic losses occur as a result of disturbances of the flow caused by equipment mounted in pipes and accessories that change the direction of the air flow path and area. Inside this definition the "local pressure losses" or "pressure losses of the section" are included. The loss in a section is defined as the mean loss of total pressure sustained by the stream in passing through the particular section. The loss in a section is given in dimensionless form by the ratio of the pressure loss in the section and the dynamic pressure at the entrance of the section [21]. For a typical "local" section this is given by:

$$K_l = \frac{\Delta P_l}{\frac{1}{2} \rho_l v_l^2} \qquad (3)$$

Where ΔP_l is the local pressure loss; ρ_l flow local density; v_l local mean speed of the flow. The summation of the pressure losses in the wind tunnel components, i.e. the total pressure drop (ΔP_l) along the wind tunnel sections, will be the pressure rise required by the fan. A summation of the pressure loss calculation of the wind tunnel components at a speed of 20 m/s indicated a necessary pressure increase of approximately 212 Pa. Most pressure loss coefficients are taken from engineering handbooks or manufacturer specifications. The remaining coefficients are explained in the following sections.

2.3.1 Settling Chamber

The settling chamber has a total length of 2.8 m. The settling section serves the purpose of straightening the flow as well as attenuating some sound disturbances in the incoming flow. The settling section houses the plenum chamber, honeycomb and screens. These components aid to increase the quality of the flow. The settling chamber should be long enough for the incoming turbulence to dissipate, while minimizing the boundary layer growth.

The fans feed a plenum chamber, 1 m long with a safety screen at the end. The main objective of this element is to break the angular component of the flow coming from the 4 fans. Each fan is enclosed by one of these chambers. They are boxes of wood, the same material of the tunnel's walls. The plenum chambers are square boxes of 1.12 m x 1.12 m, with external walls of 20 mm of width and internal walls of 10 mm of width. The plan view presented in **Figure 2** shows them.

A safety screen is positioned at the end of the plenum chambers. It provides the necessary protection for the fans and it makes the flow velocity profile in the settling chamber more uniform and reduces overall turbulence. Based on the wire Reynolds numbers given by Pope and Rae [21] for standard air, a safety screen with a mesh aperture of 5 mm and a wire diameter of 2 mm was selected. More detail about wire meshes will be explained later.

A honeycomb is installed to straighten the flow as well as to attenuate some high frequency noise. It removes swirl from the incoming flow and minimizes the lateral variations in mean velocity [22]. It breaks up the large scale eddies in the incoming flow and also aids in reducing the magnitude of the lateral turbulent velocity fluctuations.

Honeycombs come in different shapes, including circular, square, hexagonal, etc. Among these, hexagonal is usually the cross-sectional shape of choice, as it has the lowest pressure drop coefficient [23]. The ideal length to hydraulic diameter ratio of the honeycomb cells should be between 5 and 10. In the facility under discussion the length is equivalent to 10' cell diameter D_h. A longer honeycomb section would lead to a larger boundary layer growth and hence leads to more pressure drop.

Mehta & Bradshaw (1979) also states that the cell size should be smaller than the smallest lateral wavelength of the velocity variation, which is roughly equivalent to 150 cells per settling chamber diameter. The dimensions of each cell are given in Figure 3. The individual passages in the honeycomb have a diameter D_h of 5 mm and a honeycomb thickness in flow direction L_h of 50 mm. The maximum Reynolds number based on the cell hydraulic diameter should be 6521, indicating that the flow is turbulent. The honeycomb section is constructed of aluminum, for the sake of structural rigidity. The honeycombs have to be cleaned periodically to prevent dust from clogging the cells.

Some specific data for losses in honeycombs are given by [24, 25, 26]. For honeycombs of the types shown in figure 3.1 of [21] with the ratio between thickness in the flow direction (L_h) and hydraulic diameter of a honeycomb cell (D_h) equal 6.0 and equal tube areas, the value of the honeycomb loss coefficient (K_h) are found to 0.3, 0.22 and 0.2. We select a K_h equal 0.2 because of the type of honeycomb chosen.

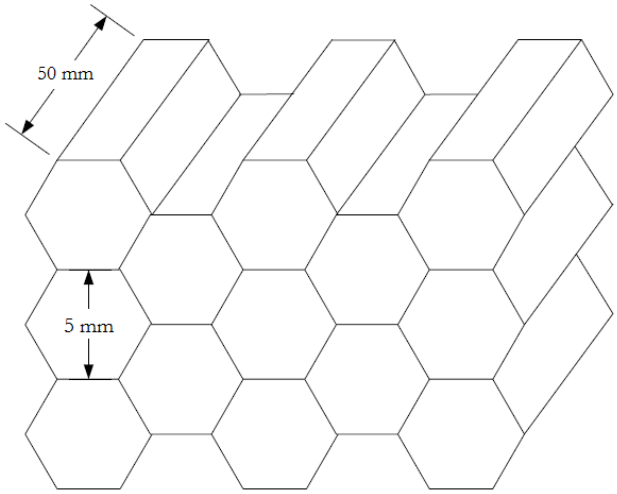

Figure 3: Schematic of the honeycomb section.

Two turbulence control screens with mesh aperture of 1.81 mm and wire diameter of 0.5 mm were installed upstream the honeycomb. Applying the design guidelines given by Mehta and Bradshaw [22], the distance between screens is about 0.2 cross section diameters.

The safety screen is chosen to provide the necessary protection for the fan. It represents a significant elemental loss due to the fact that it is located in a relatively high speed part of the circuit. The others screens serve other purposes, like turbulence control for the flow conditioning screens at the nozzle entrance. The energy loss aspects of a screen will be discussed [21].

Pope & Rae (1984) develop a head loss analysis for various sections. The first analysis was based on this handbook. Each section was treated with parameters and equations presented by previous researchers. Two basic parameters are used to characterize a screen. This are the porosity "β", and the wire Reynolds number $R_{ew} = \rho.v.d_w / \mu$. A third parameter, the "mesh factor" K_{mesh} is used to differentiate between smooth and rough wire (or whatever the screen material may be). Porosity is a funtion of wire diameter and weave density. It is also dependent on geometric factors, but it is rare for other than a square weave to be used. Let d_w be the wire diameter and w_m the width of one square mesh cell. Then the mesh density $\rho_w \equiv 1/w_m$ and the porosity is related to these by:

$$\beta_s = (1 - d_w \rho_w)^2 \qquad (4)$$

The complement of screen porosity, screen solidity $\sigma_s = 1 - \beta_s$. Porosity would be zero for a solidly packed weave and one in the limit of a vanishing screen. Typical values for wind tunnel screens are in the range of 0.5-0.8. A middle value of this range was considered to make the first analysis before buying the wire meshes.

The wire Reynolds number is typically very low compared to other Reynolds numbers encountered in the wind tunnel. Wire Reynolds number for safety screens could be up to a few thousand. For the turbulence control screens, values are likely to be only up to a few hundred (these criteria were adopted).

Mesh factors are given by [27]. We assumed the value of 1.3 for average circular metal wire.

The expression to approximate the local loss coefficient for a screen are

$$K_m = K_{mesh} K_{Rn} \sigma_s + \frac{\sigma_s^2}{\beta_s^2} \qquad (5)$$

where the reference [28] gives, for $0 \leq R_{ew} \leq 400$,

$$K_{Rn} = \left[0.786.\left(1 - \frac{R_{ew}}{354} \right) + 1.01 \right] \quad (6)$$

and, for $R_{ew} \geq 400$

$$K_{Rn} = 1.0 \quad (7)$$

Based on these parameters, the energy loss in each screen could be estimated.

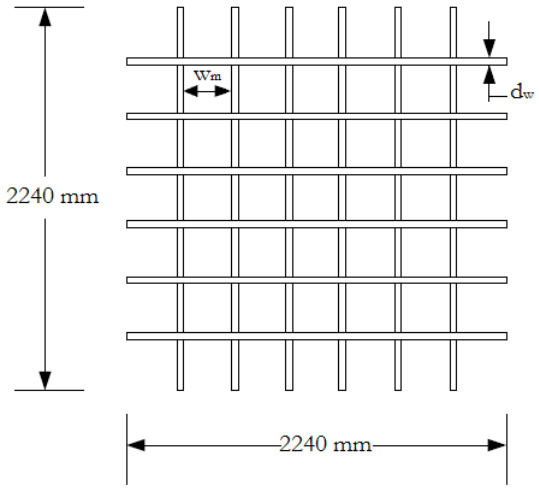

Figure 4: Schematic of the screen design

2.3.2 Contraction

The final component that reduces the turbulence intensity is the contraction nozzle. This reduction can be estimated by $1/N^2$, with $N = S_{in}/S_0$ being the contraction ratio [23]. The contraction accelerates and aligns the flow towards the test section. The design of the tunnel inlet contraction is important to provide a good flow quality in the test section. The size and shape of the contraction also dictates the final turbulence intensity levels in the test section [29]. The length of the contraction should be small to minimize the boundary layer growth. The flow leaving the contraction should be uniform and steady.

The shape and length of the 4-Winds OJWT contraction is not conventional. It has a frustum shape with the largest base of 2.24 x 2.24 m and the smaller of 1.5 x 1.5 m. The total length of the contraction is 1 m. The shape was selected based on the budget and the available space.

Founded in the analysis given by (Pope & Rae, 1984) about nozzle loss coefficient a loss of 3 % of the total losses in the circuit of the wind tunnel was applied. Special attention has been given to this component and some conclusions have been developed throughout this work.

2.3.3 Test Section

The test section is approximately 1.5 m in height by 1.15 m in width by 3 m in length. The maximum velocity of the flow in the test section is set at 17 m/s. The maximum Reynolds number calculated based on the hydraulic diameter of the test section is 1.96×10^6. It is also essential to have low values for the blockage ratio. It is often addressed as a function of frontal area of the object and the wind tunnel's cross section. Taking into account the frontal swept area of a small urban VAWT, i.e. around 0.5 m x 0.5 m, and knowing the cross-section area of the test section, a blockage ratio of around 0.11 was obtained.

2.3.4 Fans

The air in the tunnel is blown by fans, they must be dimensioned to reach the desired conditions in the test section, as well as the elements that conform it to reduce losses and maintain a stable flow. In general, the important data to acquire the fan are; the flow of air to be moved and the maximum static pressure to overcome.

The air flow is the volume of the flowing fluid per time unit, this parameter can be determined if the section and the tunnel entry speed are known.

With this concept in mind, we begin the calculation starting from the equation of continuity for an incompressible fluid,

$$A_1 v_1 = A_2 v_2 \qquad (8)$$

Where A and v, are the area and velocity in two positions of the duct. Taking A_1 as the output section of the contraction, A_2 the input section of the contraction, and v_2 the velocity to be reached in the test section, we can estimate v_1 which will be the velocity at the entrance of the tunnel.

To determine v_1 the following are defined:

a. A test section A_1 de 1.5 m x 1.5 m.
b. A maximum speed in the test section v_2 de 20 m/s.
c. An entrance section A_2 de 2.25 m x 2.25 m.

The dimensions of the test section were established taking into account conditions such as: the space available in the laboratory where the tunnel would be built and the blocking area necessary for the good performance of the measurements in the wind tunnel.

The blocking area, which is defined as the ratio between the turbine sweeping section and the test section is generally expressed in percentage. Based on the available literature, the usual blocking area is between 5% and 14%.

The entrance section was defined mainly in terms of the space available in the laboratory where the tunnel would be built.

Knowing this data, it is possible to know the value of v_1 = at 9 m / s.

Given A_1 and v_1 it is possible to know the flow rate Q from the following equation:

$$Q = A_1 v_1 \qquad (9)$$

The value of Q results 162000 m^3/h.

The maximum static pressure to be overcome is the sum of all the load losses in each tunnel element. This can be expressed by the following equation:

$$\Delta P_{total} = \sum K_1 . \left(\frac{\rho . v_1^{\,2}}{2} \right) \qquad (10)$$

Being ΔP_{total} the total load loss, K_l the load loss coefficient in each element, v_l the local velocity of the element and ρ the density of the air in the city of Tarragona, Spain.

Below, the calculation is presented in each section of the tunnel.

Settling Chamber

The losses occurring in the settling chamber are mainly due to friction and the loss coefficient is given in [23]

$$K_{SC} \quad \frac{f_{SC} L_{SC}}{D_{SC}} \left(\frac{D_{TS}}{D_{SC}}\right)^4 \qquad (11)$$

where f_{SC} is the friction factor, L_{SC} is the total length of the settling chamber, D_{SC} is the hydraulic diameter and D_{TS} is the hydraulic diameter of the test section. The friction factor for a fully turbulent flow f, is given by Haaland equation,

$$\frac{1}{\sqrt{f}} \quad -1.8 log_{10}\left[\frac{6.9}{Re_D} + \left(\frac{\varepsilon/D}{3.7}\right)^{1.11}\right] \qquad (12)$$

where Re_D is the Reynolds number based on the hydraulic diameter and ε is the surface roughness. ε = 0.0016 m (corresponding to a fairly rough surface), as the surface roughness of the individual components cannot be known beforehand. Usually, settling chamber losses are a very small fraction of the total loss.

The velocity at the entrance of this section is 9 m/s (for the max tunnel speed of 20 m/s) and the hydraulic diameter is 2.24 m giving a Reynolds number of 1.26 10^6. Assuming a value for ε/D = 0.0007 m and substituting into **Equation (12)** we obtain f_{SC} = 0.018. The length of the settling chamber is 2.8 m and the test section hydraulic diameter is 1.5 m. Substituting these values in **Equation (11)** yields a value of K_{SC} = 0.005.

a. Screens and honeycomb

The losses across safety and turbulence screens have been calculated by **Equation (5).** We have used three screens in the current design. The value *K* for the safety screen (K_{sm}) is thus 1.56 and the *K* value for each turbulence screens (K_{ml}) is 0.98.

The loss across the honeycomb section is given by Reference [21] and it was described in **2.3.1 section**. The value of the honeycomb loss coefficient (K_h) is 0.2.

b. Contraction

The losses occurring in the contraction are predominantly due to frictional effects. A reasonable approximation for nozzle loss coefficient that was originally given by Wattendorf in 1938 and is described in Reference [21] as

$$K_{nl} \quad \frac{0.32 f_{avg} L_{nl}}{D_{TS}} \tag{13}$$

where f_{avg} is the average value of the friction factors at the entrance and exit of the nozzle and L_{nl} is the total nozzle length. According with Reference [21], the loss in the nozzle is typically of the order of 3 % of total losses in the circuit, so this consideration was applied.

c. Test Section

Frictional losses predominate in the open jet test section due to the jet shear layer, and the loss coefficient is given by [23]

$$K_{TS} \quad \frac{f_{TS} L_{TS}}{D_{TS}} \tag{14}$$

where L_{TS} and D_{TS} are the length and hydraulic diameter of the test section respectively. The friction factor f_{TS} has a value of 0.08 for a cylindrical open jet test section [23]. The length of the test section considered was of 2 m and therefore the loss factor is 0.11.

The results from the fan loss calculation are given in **Table 2**. From the table, K is the pressure loss coefficient and ΔP_l is the pressure loss across the individual wind tunnel component.

It can be observed from the table that the maximum loss occurs in the safety screen. Other remarkable losses occur across the turbulence screens. The total loss factor is the sum of the individual loss coefficients, and has a value of approximately 4 that translates to a value

of 212 Pa of pressure that the fan has to overcome. Taking a factor of safety of 1.35, a value of approximately 300 Pa of pressure was considered.

Component	**K**	**ΔP (Pa)**	**% Total loss**
Settling Chamber	0.005	0.24	0.11
Safety screen	1.56	75.18	35.48
Honeycomb	0.2	9.64	4.55
Turbulence screen 1	0.98	47.23	22.29
Turbulence screen 2	0.98	47.23	22.29
Contraction	0.13	6.26	2.95
Test section	0.11	26.18	12.36
		Total	100

Table 2: Results of the wind tunnel head loss calculation

In a simplified way, the open circuit wind tunnel, open test section and blow-up can be seen in the figure. The direction of the air circulation is indicated with blue inlet and red outlet arrow. Each pressure drop calculation section is also identified; the calculation was started in the test section, i.e. the so-called "0".

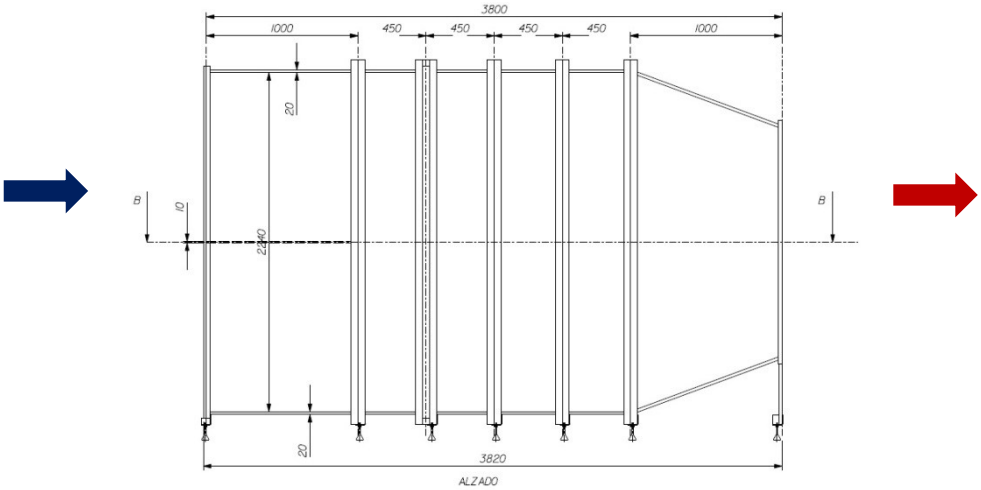

Figure 5: List of local sections where the pressures have been estimated.

This is the tunnel that is considered as a starting point to then reach the most favourable design conditions, finally obtaining a prototype for the construction.

2.4. Numerical Simulation

A numerical simulation was performed in order to predict the behavior of the air flow which passes through all sections of the tunnel.

GAMBIT graphical user interface (GUI) to create and mesh the geometry was used. It is a simple, integrated preprocessor for CFD analysis. The geometry construction, mesh generation, meshes quality examination and boundary zone assignment was carried out in this software.

Figure 6 shows one of the first geometries made. The 2 D plane presents a lateral view with principal dimensions in millimeters. The 3 D view (isometric view) illustrates the screens and the honeycomb meshed. Their forms can be seen in the following illustration.

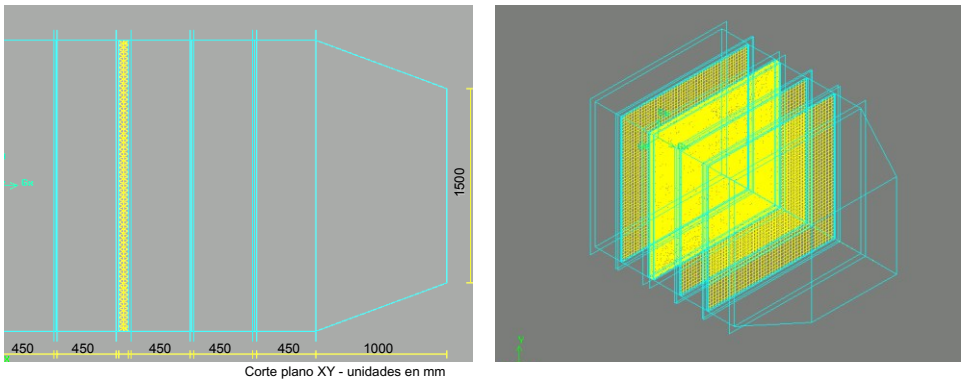

Figure 6: Left, 2 D plane of a lateral view with principal dimensions in millimeters. The 3 D plane (isometric view) illustrates the screens and the honeycomb meshed.

Local and global meshing has been applied. After that, the examination of the mesh has been made. Then, the zones were assigned and boundary layers were defined. Finally the mesh was imported and the Gambit session saved for working in Fluent.

Once the tunnel mesh geometry was generated, the computational domain consists of the whole tunnel sections (**Figure 6**) and a section where the jet flows is expanded freely.

An unstructured 3 dimension mesh was used for the domain meshing. As a mesh independence test, different sizes of meshes have been simulated. A mesh with a total of 945000 mixed elements in the computational domain was selected. Meshes with more elements presented same results and major cost of time. The isometric view of the flow domain is shown in **Figure 7**.

Velocity-inlet boundary condition was applied at the entrance of the domain and the following step as the selection of the Components as Velocity Specification Method.

Then, the Cylindrical Coordinate System was chosen to define the velocity vector at the inflow boundary. In this instance, the Axial Velocity and the Angular Velocity have been specified. Considering steady and incompressible flow of fluid through the tunnel, the Axial-Velocity was estimated by the equation of continuity and a value of 9 m/s was obtained.

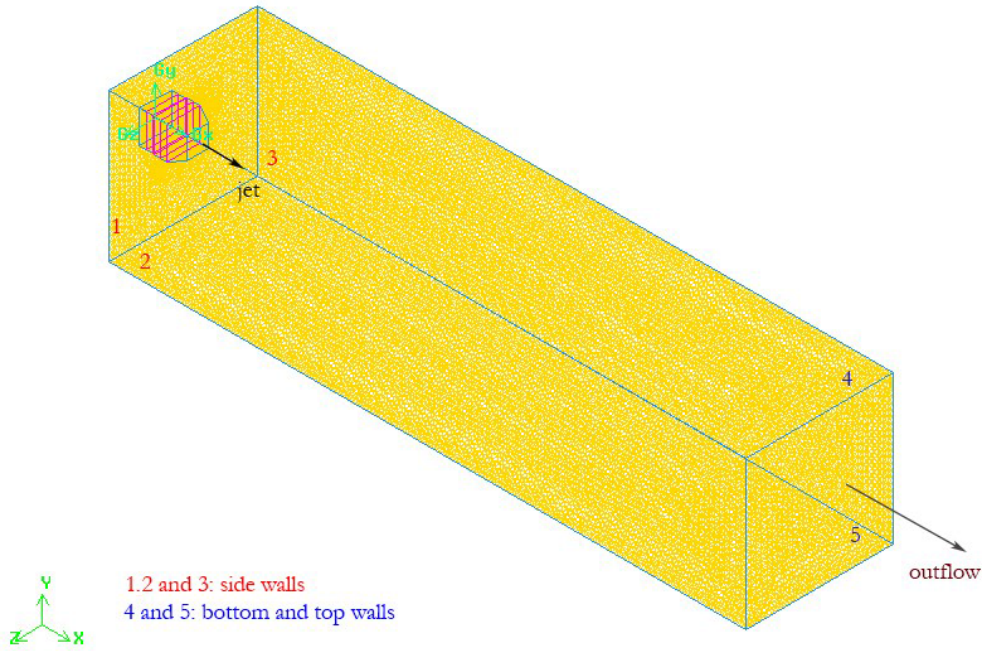

Figure 7: Full flow domain.

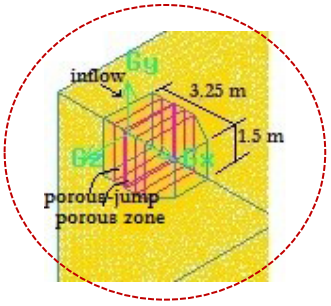

Zoom of wind tunnel geometry

Simulations with one inlet and four inlets were carried out, i.e. supposing two configurations, with one axial fan or with four axial fans. In both cases, i.e. with one axial fan and four axial fans, the axial-velocity indicated was 9 m/s as was explained before, the angular-velocities have been defined using empirical calculation considering the relation between linear velocity and the radius of the axial fan. A value of 56.55 rad/s was used for one axial fan of 1 m of radio and a value of 113 rad/s for each fans of 0.5 m of radius. The outflow boundary condition was imposed at the domain exit. The domain contains the settling chamber components (safety screen, honeycomb and two turbulence screens), then the contraction and finally an extended test section domain. To obtain the most appropriate wind condition, the downstream boundary is extended approximately 33 meters from the tunnel outlet. The components of the settling chamber were simulated according to: Screens as porous-jump boundary conditions; Honeycomb as a volume and porous zone conditions. The steady state, 3-D Navier Stokes equation was solved using the shear-stress transport (SST) k-ω model for a maximum test section velocity of u_{ts} = 20 m/s. ANSYS Fluent 12.0 Theory Guide presents the mathematical model in its chapter where provides theoretical background about the turbulence models available [30].

Contours of "x" component at the velocity vector along the domain centre plane (xy plane), simulated with four entrances is shown in **Figure 8** and with one entrance is shown in **Figure 9.**

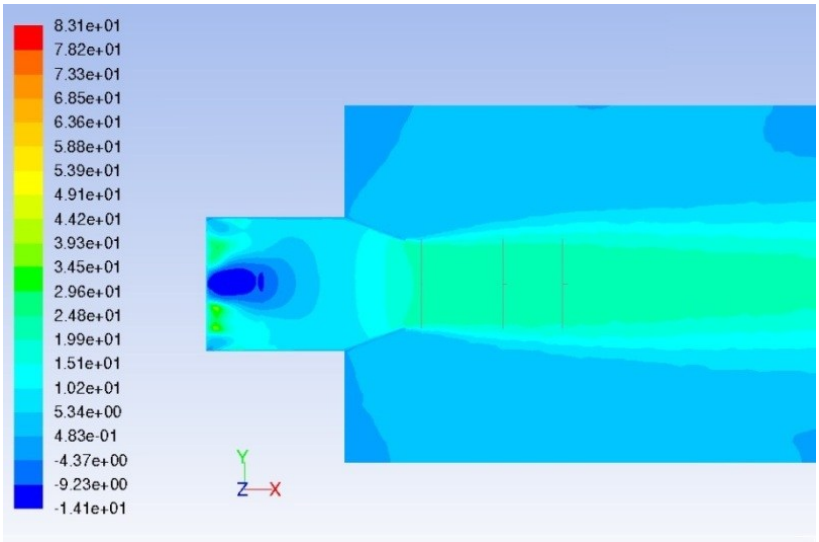

Figure 8: Centre plane of contours of x component velocity along tunnel and part of extended domain with four axial fans.

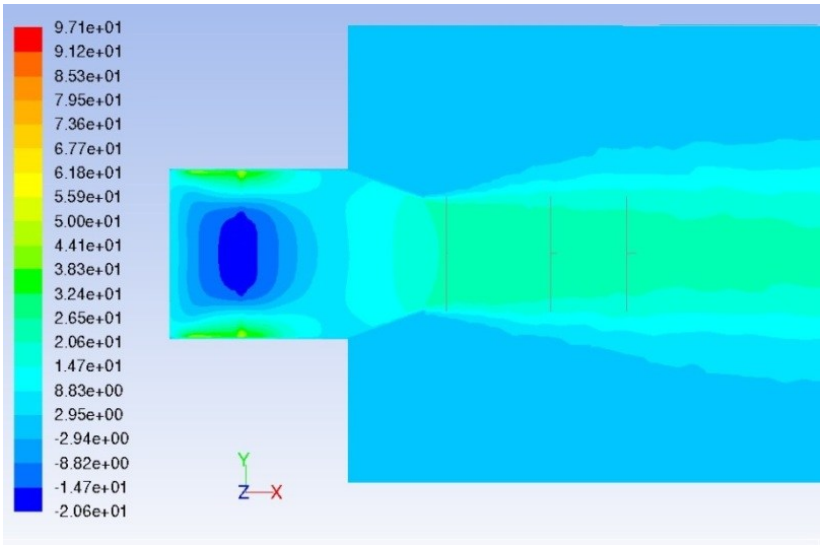

Figure 9: Centre plane of contours of x component velocity along tunnel and part of extended domain with one axial fan.

The results indicate that the flow is stagnant in the first zone of the settling chamber and this is more pronounced with one fan. However, the flow expanded and accelerated in the contraction in both cases. Then the x component at the velocity increases at the test section area and its value is in the order expected (≈ 0.3 m).

This figure also presents grey lines in three different positions of the extended domain, i.e. in the test section area. These grey lines are drawn on the "yz" plane. **Figure 10** shows the

contraction mesh and the grey lines where the characteristics of the flow were analyzed. The first ones were positioned at approximately 0.3 m from the nozzle exit, the second and third at approximately 2 m and 3 m respectively.

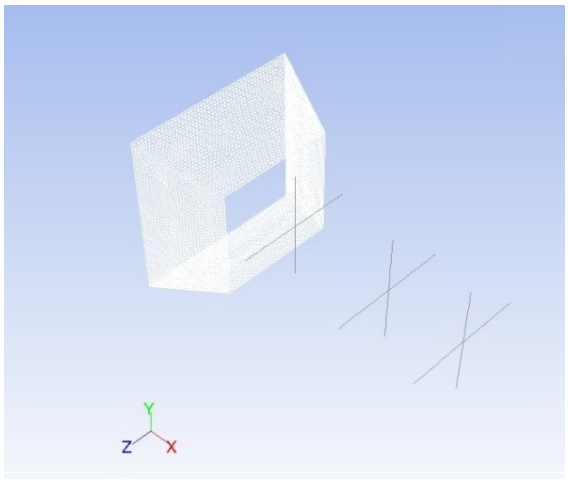

Figure 10: Contraction mesh and points analyzed along y-axis and z-axis.

The numerical velocity profiles at vertical and horizontal planes are analyzed**.** Next figures show the x component of the velocity along y-axis and z-axis on three different positions from de nozzle exit for 4 axial fans and 1 axial fan cases.

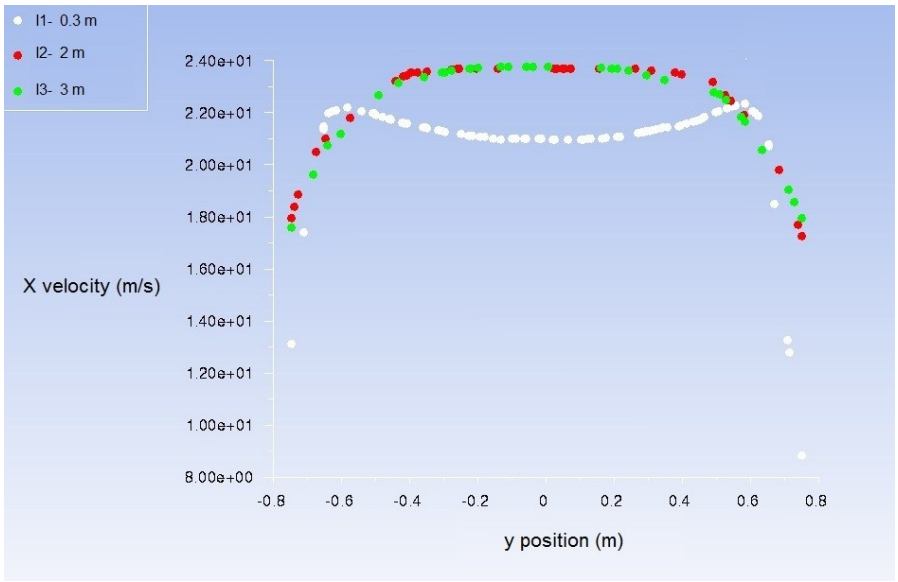

Figure 11: X component of the velocity along y-axis (4 axial fans case)**.**

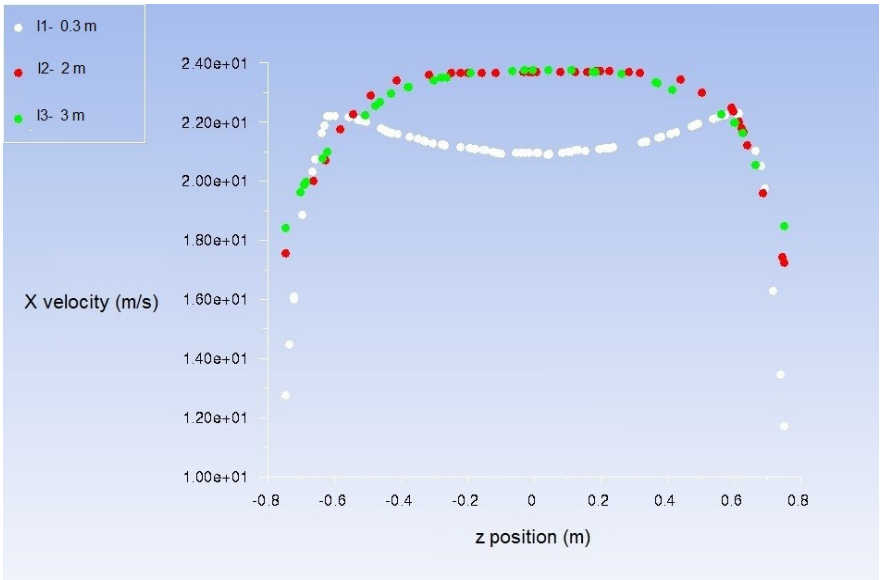

Figure 12: X component of the velocity along z-axis (4 axial fans case).

All figures present larger velocities and relatively uniform velocity profiles at 2 m and 3 m from the nozzle exit. The uniform velocity profiles have been presented from -0.4 m to 0.4 m of the test area in both cases, that is, along y and z axes. The cases with 4 axial fans show velocity profiles more uniform than cases with 1 axial fan at 2 m and 3 m from the nozzle exit.

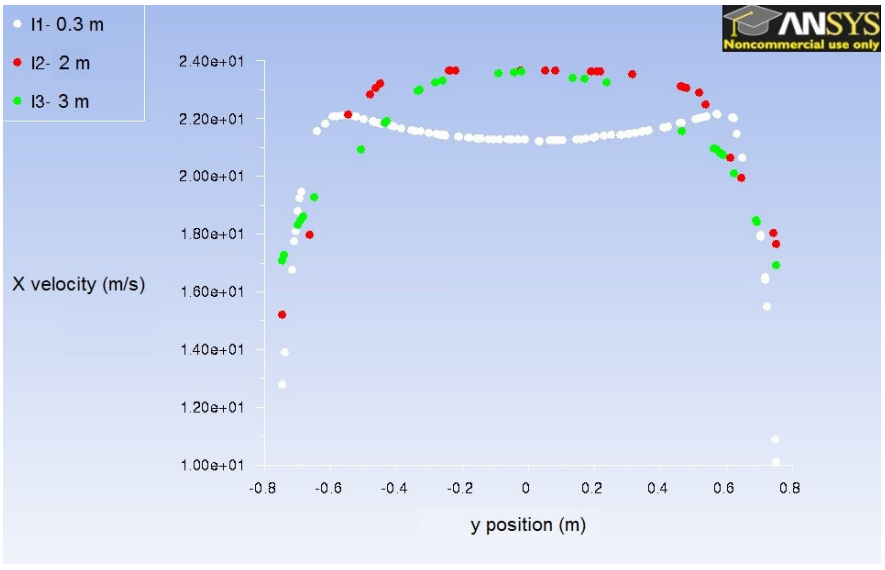

Figure 13: X component of the velocity along y-axis (1 axial fan case).

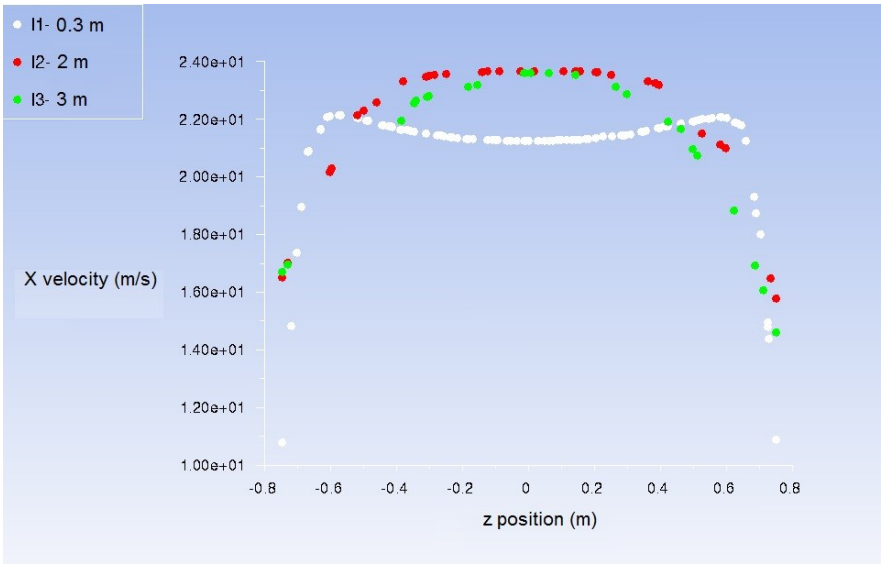

Figure 14: X component of the velocity along z-axis (1 axial fan case).

The numerical results predicted that an open jet wind tunnel equipped with a matrix of 4 axial fans and 3 screens could produce:

- Zero velocities in the middle of the matrix of the four fans.
- Uniform flow quality in a section of 0.8 x 0.8 m^2 of the jet.
- No separation of the flow along the contraction.
- Values expected of velocities at the exit of the contraction.

All these results have been improved and discussed in the course of the design, built and characterization of the new open jet facility of Tarragona. The most significant change was the implementation of a plenum chamber of 1 m in order to break the angular component of the flow coming from the fans.

Figure 15 illustrates a comparison between numerical results of the normalized mean velocity profiles of the x-component at x = 0.3 m, z = 0 and experimental results of the normalized mean velocity profiles of the *u*-component at x = 1 m, z = 0. It can be seen that velocity profiles present similar trend.

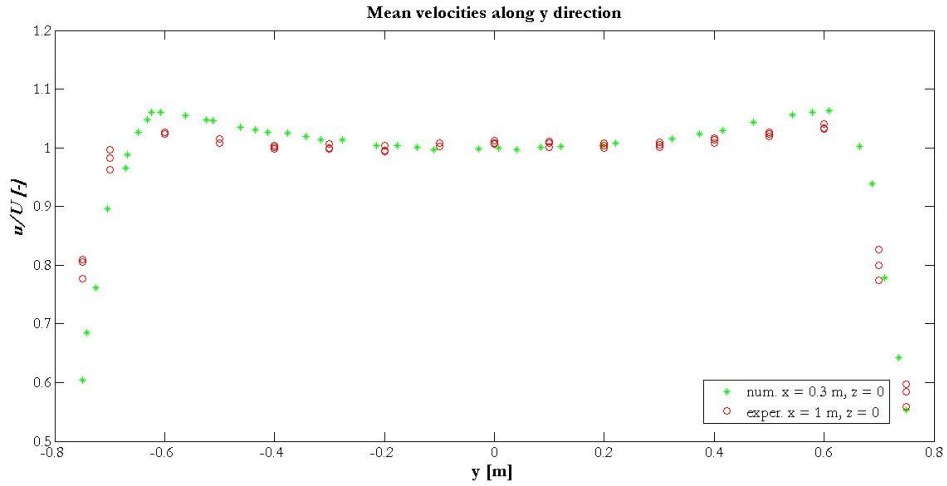

Figure 15: Normalized numerical velocity profiles (x-component) along the horizontal y-direction at x = 0.3 m and z=0 and normalized experimental velocity profiles (*u*-component) along the y-direction at x = 1 m and z = 0 with the false ceiling.

Analogous results can be seen in **Figure 16**, where numerical velocity profiles (x-component) along the vertical z-direction at x = 0.3 m, y = 0 and experimental velocity profiles (*u*-component) along the z-direction at x = 1 m, y = 0 with the false ceiling had been represented.

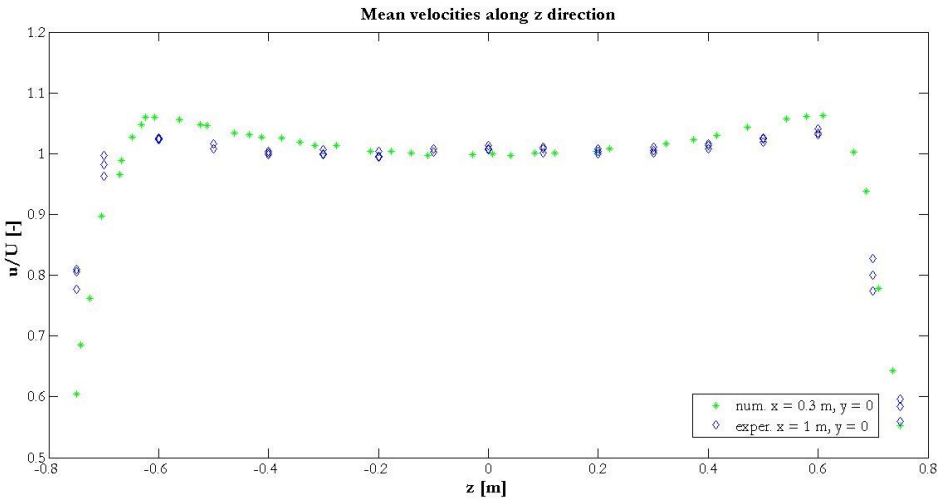

Figure 16: Normalized numerical normalized velocity profiles (x-component) along the vertical z-direction at x = 0.3 m and y = 0 and normalized experimental velocity profiles (*u*-component) along the z-direction at x = 1 m and y = 0 with the false ceiling.

Chapter 3

CHARACTERISTICS OF THE WIND TUNNEL COMPONENTS

This chapter discusses the fabrication of the wind tunnel components. A brief description about material selected and design aspects are also provided. The 4-Winds OJWT tunnel is modular and it can be disassembled. The components will be described in the direction of the flow: fans, plenum chamber, flow straighteners and conditioning elements and finally the contraction.

3.1 Fans

The 4-Winds Open Jet Wind Tunnel has four identical axial fans (long cased variable pitch blades type) arranged in a two by two matrix. The fans can deliver a maximum flow of 61590 m^3/h. The fans can be operated at several rpm settings using a Toshiba Model VF-FS1 variable frequency drive. Four 7.5 kW motors which operate at a maximum speed of 1440 rpm, are used to drive the tunnel. The front and back views of the fan matrix are shown in **Figure 17** an**d Figure 18,** respectively.

Figure 17: Front view of the fans.

Figure 18: Back view of the fans.

Mechanical vibrations from the drive fan must be isolated from the main body of the tunnel. The matrix of the fans is attached firmly to a strong iron structure, which is separated of the body of the tunnel by a rubber sheet. This rubber sheet covers all contact area between the body of the tunnel and the fans matrix in order to prevent the air leak and bring a soft contact to decrease the mechanical vibrations as much as possible. The base of the matrix of the fans also has non-slip feet. It has approximately 2.5 m^2 in order to guarantee the distribution the weight on surface required by the safety standards of the institution.

3.2 Plenum chambers

Each fan discharges into its plenum chamber, each with a length of 1 m and ending in a safety screen which acts as a flow straightener element. Plenum chambers are the first module of the tunnel. The 4-Winds OJWT consists of six modules, all detachable from each other and also detachable individually so they can enter the door of the laboratory where the tunnel was located. The modules were fabricated in phenolic plywood of 20 mm thick.

The 4-Winds OJWT was designed and built by a Naval Architect and Naval Technicians with years of experience in engineering and construction.

The main objective of the plenum chambers is to break the angular component of the flow coming from the fans. They are square boxes of phenolic plywood with a 1.12 m x 1.12 m surface, with external walls of 20 mm of width and internal walls of 10 mm of width. The front and back views are shown in **Figure 19.**

Figure 19: Front and back views of plenum chambers.

3.3 Flow straighteners and conditioning elements

The next modules of the 4-Winds OJWT are the straightener elements. They consist of three grids and a honeycomb to provide uniformity at the velocity profile and the turbulence of the incident flow. Based in Reference [22] the space between screens is about 0.2 diameter of the settling chamber. Screens and honeycomb are located into wooden frames. Screens and honeycomb frames rest on lanes and they are clamped by drawbolts, so they can be withdrawn easily for cleaning and maintenance.

The porosity of the safety screen and the turbulence control screens have been defined by the wire diameter and the width of one square mesh cell. These parameters have been found by wire Reynolds numbers suggested in the literature review. The material of the

meshes is inox AISI 304. **Figure 20** shows pictures of the safety and the turbulence control screens.

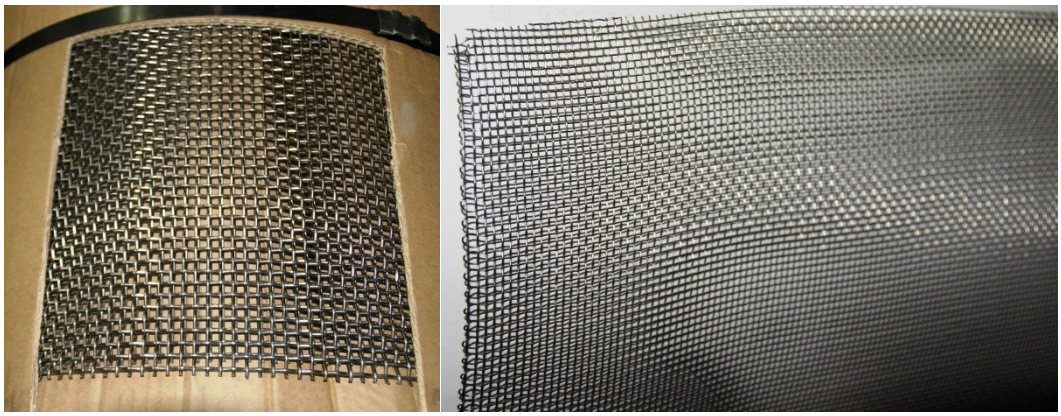

Figure 20: Safety screen and turbulence control screen pictures.

The honeycomb material is aluminium, this material gives structural rigidity. The cell configuration has approximately the form of an hexagon. It is very impact sensitive, despite their rigidity and must be handled carefully. The honeycomb thickness is 50 mm, cell size 5 mm and the aluminium foil density is around 42 kg/m^3. **Figure 21** shows a picture of the honeycomb wooden frame removed from the settling chamber, in order to show that it can be removed for cleaning.

Figure 21: Honeycomb wooden frame removed for cleaning.

3.4 Contraction

The contraction is the last module of the 4-Winds OJWT. The contraction has a frustum shape, with the largest base of 2.24 x 2.24 m and the smaller of 1.5 x 1.5 m. The total length of the contraction is 1 m. The shape was selected based on the budget and the available space.

Photographs of the front and back views of the wind tunnel painted are shown in **Figure 22** and **Figure 23**, respectively.

Figure 22: Front photo of the 4-Winds OJWT.

Figure 23: Back photo of the 4-Winds OJWT.

The 4-Winds OJWT was located in a teaching laboratory, so that a safe circulation of the wind tunnel operator and students of the Rovira i Virgili University must be guaranteed. The security mesh of the fans and the safety bars on the basis can be seen in **Figure 23**.

Chapter 4

EXPERIMENTAL METHODS

This chapter describes the experimental setups and procedures for the experiments undertaken to characterize the wind tunnel. The experiments include freestream flow uniformity and turbulence measurements with different instruments. These experiments were carried out twice because the test section area was modified. A description of the traversing mechanism of the measurement instruments is also provided.

4.1 Flow uniformity and turbulence measurements

Flow uniformity and turbulence measurements were made using four NPL 8 mm pitot tubes and a Constant Temperature Anemometer (CTA) system.

The pitot tubes measure the total pressure. They are used to calibrate the single hotwire probes of the CTA system and to measure the velocity in reference points during all tests. Pitot tubes had been calibrated under laboratory accreditation requirements of the United Kingdom Accreditation Service (UKAS). The measured data was acquired using four Setra C239 differential pressure transducers calibrated by NIST RPT 1500129433 and a NI compactDAQ-9172 chassis with Analog Input Modules NI 9215. The velocity is calculated considering the relation given by the certificates of the calibration (See **Equations 15-18**)

Air velocity (mps) $$.291\sqrt{\left(\frac{1013.25}{Pb} * \frac{T+273}{293} * \frac{10^5}{10^5+Ps} * \frac{h}{K}\right)} \quad (15)$$

Which, assuming standard conditions,

$$.291\sqrt{\frac{h}{K}} \quad (16)$$

$$.291\sqrt{kh} \quad (17)$$

$$.291 * \Gamma\sqrt{h} \quad (18)$$

Where:

Pb is the Barometric Pressure in mBars

T is the temperature in degrees Centigrade

Ps is the Pitot Static Pressure in Pascals

h is the Pitot Static Pressure in Pascals

K is the Magnification Factor of the Pitot

k and Γ are Pitot constants.

Figure 24 shows the location of one of the pitot tubes to calibrate the hotwire probes of the CTA system. Different distances and positions between pitot tubes and hotwire probes have been carried out in order to find an appropriate place where the signals can be reproduced. The optimum distance between hotwires probes and pitot tubes was set to 60 mm.

Figure 24: Pitot tubes and hotwire probes positions during calibration measures.

Other measure instruments used to carry out the calibrations were:

A) The humidity and temperature probe HMP155 was calibrated by comparing the readings of the instruments to the standards of the manufacturer. The reference humidity

was calculated from dewpoint temperature and temperature readings with the exception of the driest condition that was measured as relative humidity. Dewpoint temperature was measured at 373 LHX dewpoint meter. Temperature and relative humidity were measured with two factory working standards. At the time of the shipment, the instrument described above met its operating specifications. The 373 LHX dewpoint meter was calibrated at the National Institute of Standars and Technology (NIST). The temperature readings of the factory working standards have been calibrated at an ISO/IEC 17025 accredited calibration laboratory (FINAS), Vaisala Measurement Laboratory (MSL) by using MSL working standards treaceable to NIST. The relative humidity readings of the factory working standards have been calibrated at the Vaisala factory by using 373 LHX dewpoint meter.

B) Barigo barometer, calibrated in accordance with the conditions of acredditations granted by Entidad Nacional de Acreditación (ENAC). ENAC is one of the signatories of the Multilateral Agreement of the European Cooperation for Acreditation (EA) and the International Laboratories Accreditations Cooperations (ILAC).

It is necessary to clarify that the barometer has been placed in a semi-open box in order to guard it from the flow of the tunnel. On the other hand, the temperature and humidity probe has been located in side of the jet region.
The calibrations were made in the potential core before and after each characterization. The potential core is close to the nozzle [31]. In this zone the turbulence intensities are less than 1.3 % in the 4-Winds OJWT.

The CTA anemometer works on the principle of convective heat transfer from a heated element to a surrounding fluid, which is related to the fluid velocity [32]. The advantage of the CTA system is that it has flat high frequency response required for turbulence measurements. Heat loss due to conduction and radiation are assumed to be minimal. In addition, the velocity and the flow properties are assumed to be constant across the length of the measurement probe.

A Disa (Model 55M10) was used to measure the mean velocities and the velocity fluctuations in the test section. The block diagram for the measurement is shown in **Figure 25**.

The measurement probe is a straight 1-D gold-plated (type 55P01) and it is 5 μm in diameter and 1.2 mm long. The probe connects to a probe support (Type 55H20) which is connected to the CTA module via a 4 m long BNC cable (Type A 1863). The CTA module contains a Wheatstone bridge, one arm of which is the measurement probe. The resistance and hence the temperature of the probe are held constant by a servo amplifier, by adjusting the current through the bridge circuit.

The hot wire probes were calibrated in a wind tunnel with a pitot static tube as the velocity reference. The calibration was carried out in the potential core as was explained before. The output from the CTA module was fed to a NI compactDAQ-9172 chassis with Analog Input Modul NI9215, which measures the voltajes. The signal from the hot wire probes and the pitot tube were sampled at 20 kHz during 60 seconds for an increasing and decreasing range of velocities.

The probes have been re-calibrated after the experiments and compared with previous calibration. The pitot static tubes used as the velocity reference were located at ≈ 60 mm from the hot wire probes as was explained before.

The flow temperature and humidity are measured with the HMP155 probe located in the potencial core close to the other probes.

The density was calculated from the flow temperature and the ambient pressure in the test section. The change in ambient pressure was found to be around 0.1 %. The static presure was measured too.

The overheat ratio for the turbulence measurements is set at 0.8 [32]. A square wave test is done prior to measurements to estimate the bandwidth for the measurement setup. The bandwidth of the system, estimated via the square wave test, was over 20 kHz for all measurements. The continuous voltage signal from the CTA module was sent to the NI compactDAQ-9172, as was explained before, without low pass-filter before to the computer.

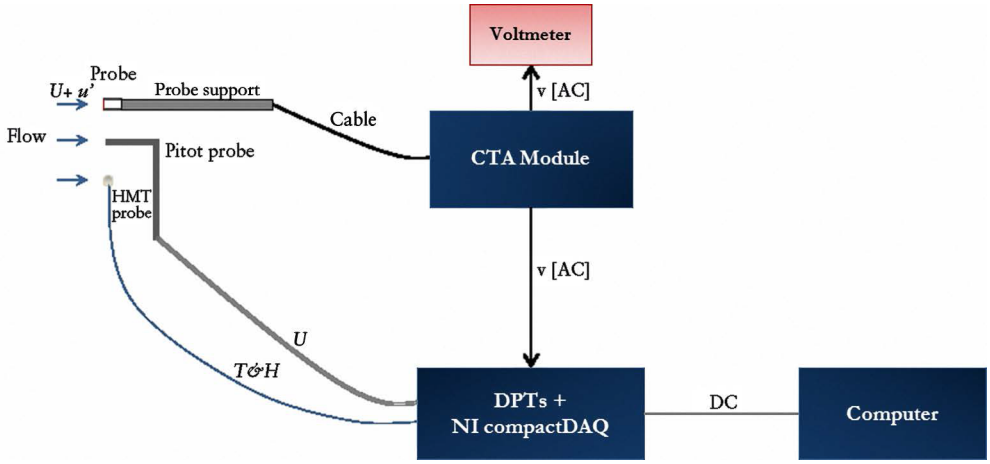

Figure 25: Hotwire measurement block diagram.

Figure 26 and **Figure 27** present pictures of the experimental instruments used to characterize the flow uniformity and turbulence characteristics on the empty wind tunnel. Differential pressure transducer of the pitot tubes as well as the NI compactDAQ-9172 are inside of a metal box in order to remove and prevent external noise that can contaminate the signal.

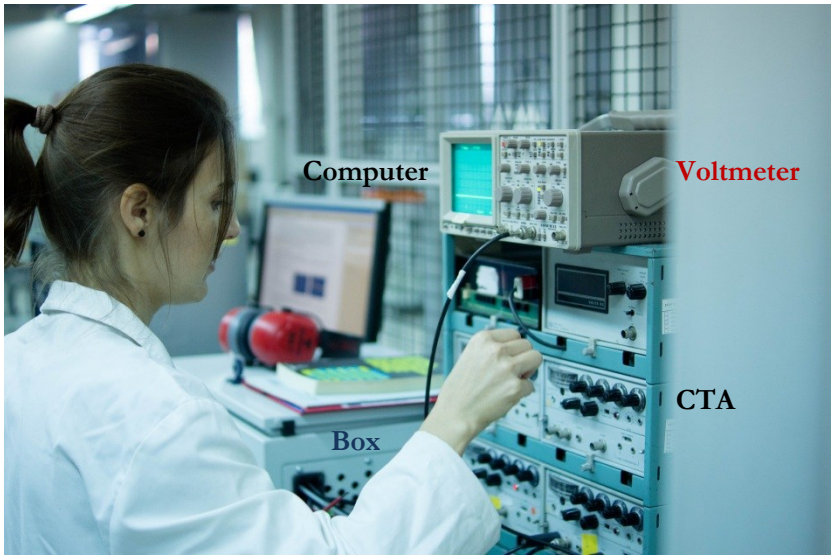

Figure 26: Background, metal box with DPTs and NI CompactDAQ.
Foreground, CTA Disa and Voltmeter.

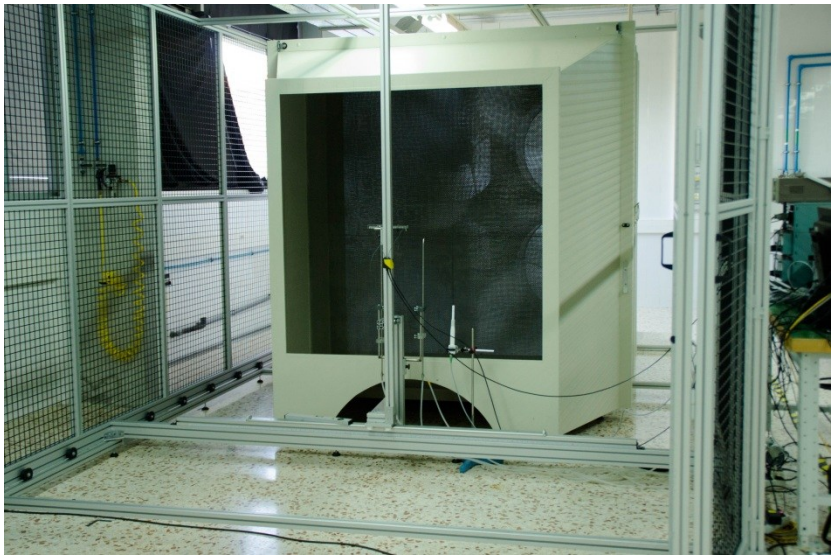

Figure 27: Instrument carriage with disposition of the experimental instruments at the exit of the nozzle.

4.2 Cup anemometer measurements

The characterization of the open test section has been completed using measurements with a calibrated cup anemometer. Having defined the uniform test section, the calibration procedure of the cup anemometer was achieved applying the procedures given by IEC 61400-12-1 of International Standards, Wind turbines - Part 12-1: Power performance measurements of electricity producing wind turbines, Reference [33] and Calibration certificate from Deutsche WindGuard Wind Tunnel Services GmbH, Varel, Denmark.

In these experiments the following instruments were used: a cup anemometer calibrated in the Wind Tunnel of Deutsche Wind Guard, Varel, Germany, four NPL 8mm pitot tubes calibrated under laboratory accreditation requirements of the United Kingdom Accreditation Service (UKAS), four Setra C239 differential pressure transducers calibrated by NIST RPT 1500129433 and an NI compactDAQ-9172 chassis with a Digital I/O Module NI 9401 and Analog Input Modules NI 9215. The signals from the pitot tubes and cup anemometer are sampled at 5 kHz during 60 seconds at every position of the defined working grid. The cup anemometer was located at y=0 and z=0 and the four pitot tubes at y = 0.4 m, z = 0.4 m; y = -0.4 m, z= 0.4 m; y= 0.4 m, z= -0.4 m and y= -0.4 m, z= -0.4 m.

Figure 28 shows the working grid of the cup anemometer calibration.

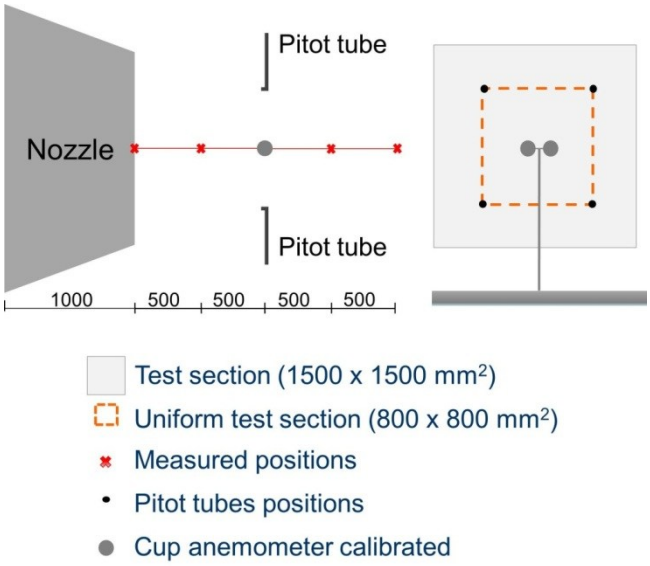

Figure 28: Working grid of the cup anemometer calibration.

Figure 29 presents a photograph of the cup anemometer measurement setup. It is possible to see the false ceiling in this picture, which is the last improvement done in this section.

Figure 29: Photograph of the cup anemometer measurement setup.

4.3 Instrument carriage

The instrument carriage provides the ability of positioning the probes in the test section. This system is supported and rests in a safety cage built to ensure the security of the operator and researchers working in the laboratory.

It is designed and built with aluminum profiles. It has a base that works as fixed rails on which the cage can move along x-axis.

The vertical aluminum profile is a guide where the probes can be moved along the y and z axes. The vertical guide is fixed before every measure from the top and from the bottom.

The positioning in all direcction, x, y and z axes is made manually and the movement is soft because the profiles rest on wheels.

The operator's console is outside the test section. **Figure 30** shows a front view of the tunnel with the frontal doors of the cage open and also the instrument carriage with all probes and the operator's console.

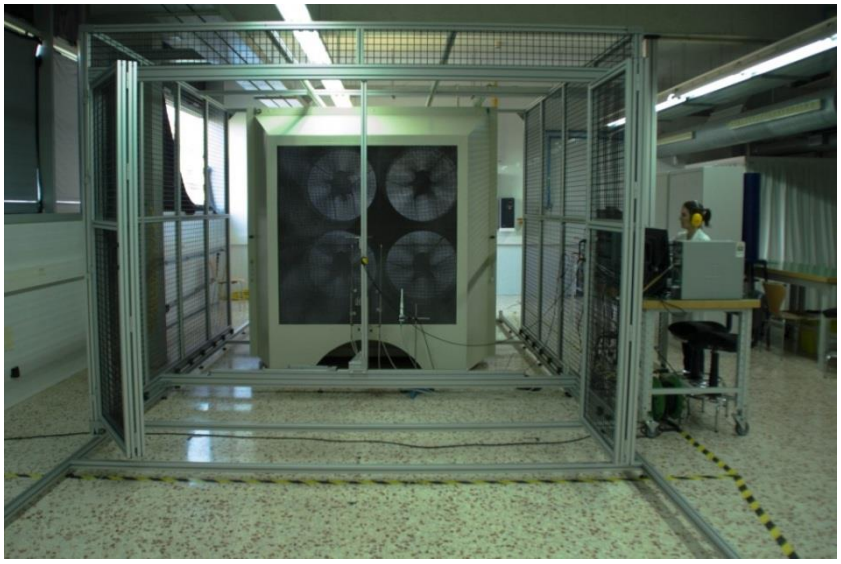

Figure 30: Front view of the 4-Winds Open Jet Wind Tunnel. Instrument carriage and operator's console.

The safety cage has served as support for the false ceiling. Therefore, this allowed us to abtain results with and without false ceiling. The results and conclusions will be discussed in the next chapters.

Chapter 5

FACILITY CHARACTERIZATION

This chapter discusses the measurements conducted in the 4-Winds open jet wind tunnel with the purpose of charaterizing its aerodnamics. A preliminary characterization of the facility has been completed for flow up to $U = 17$ m/s.

Analysis of the exit flow uniformity and turbulence characteristics using pitot tubes and hot wires as well as calibration and measurements with a calibrated cup anemometer have been carried out. The detail results of the characterization experiments are described in the next sections.

5.1 Analysis of the exit flow uniformity and turbulence characteristics

The performance in terms of flow characteristics was measured with different instruments. The origin of the coordinate system is defined at the centre of the nozzle exit plane and the x-axis is aligned with the jet axis. The orientation of the y-axis and the z-axis is horizontal and vertical, respectively (see **Figure 2**). The flow characteristics were analysed with a single hotwire probe. The signal from the straight probe 55P01 of DANTEC was sampled with 16-bit resolution and a sampling frequency of 20 kHz. It was processed to estimate the average speed U and the intensity of the fluctuations u'. A positioning system allowed the displacement of the probe along the three spatial directions. The measurements were taken at several planes parallel to the nozzle exit and along the jet axis to determine the flow uniformity and the turbulence intensities.

5.1.1 Calibration of flow velocity

Calibration establishes a relation between the CTA output and the flow velocity. It is performed by exposing the probe to a set of known velocities, *U*, and then record the voltages, *E*. A curve fit through the points (*E, U*) represents the transfer function to be used when converting data records from voltages into velocities. The calibrations were carried out in the potential core zone of the 4-Winds open jet wind tunnel with a pitot static tube as the velocity reference.

Figure 31 shows a typical curve fitting, which is a plot of test section velocity versus measured dc voltage. Measurements were made at increasing values of speeds of the tunnel as well as decreasing values of the speeds of the tunnel. The figure shows the calibrations made before (Cal_1) and after (Cal_2) every y-z plane characterization. The calibrations were completed following the manual procedure of reference [32]. In order to account for the influence of flow temperature on the measurements, the fluid temperature, T_a, was acquired, together with the CTA voltage, E_a. Then the corrected CTA voltage, E_{corr}, was calculated by equation [60] given by reference [32].

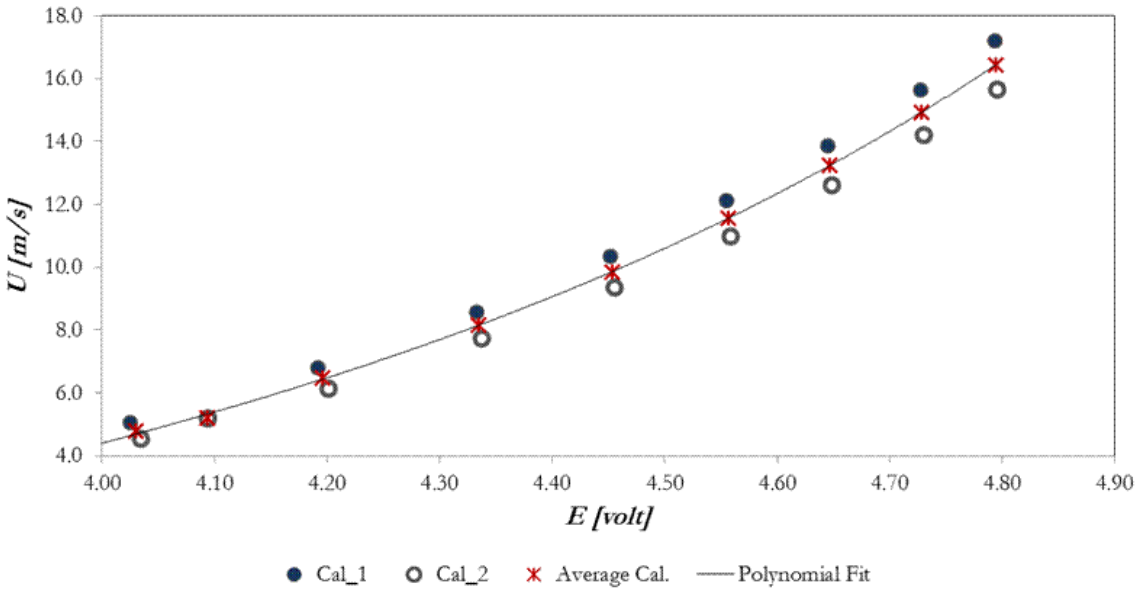

Figure 31: Calibration curve showing the plot of mean velocity vs. mean voltage.

5.1.2 Velocity profiles

The test section was characterized in two different configurations. The first configuration corresponds to the conventional location of the tunnel with the floor located at z = -1.29 m and the ceiling of the laboratory at z = 2.34 m (See **Figure 2**). In the second configuration, a false ceiling located at z = 1.29 m was installed above the test area to obtain symmetry of the flow with respect to the plane z = 0.

Figure 32 shows the time averaged scaled velocity profiles along the vertical z-direction and along the horizontal y-direction at x = 1m without the false ceiling (**Fig. 32(a)**) and with the false ceiling (**Fig. 32(b)**), while **Figure 33** shows the corresponding profiles at x = 2 m. The profiles have been scaled using the measured velocity at the center of the nozzle exit. The specific values for the three different exit velocities are 5.0 m/s, 11.0 m/s, and 14.4m/s for the profiles of **Figure 32** and 5.4 m/s, 11.0 m/s, and 15.0 m/s for the profiles of **Figure 33**. The distance between the locations of measurement is 0.1 m. Red symbols show the mean velocities along the horizontal y-direction, and blue symbols correspond to velocities along the vertical z-direction. It can be seen that the velocity profiles with the false ceiling show more uniform profiles along the y-axis. The ratio between the standard deviation (σ) and average velocities in the regions - 0.5 m $\leq$ y $\leq$ 0.5 m and -0.5 m $\leq$ z $\leq$ 0.5 m is 0.01. Note that the average velocities in the regions near z = $\pm$0.6 m and y = $\pm$0.6 m increase due to the relatively rapid contraction of the tunnel exit.

Figure 33 shows the time averaged velocity profiles normalized along the vertical z-direction and along the horizontal y-direction at x = 2 m without the false ceiling (**Fig. 33(a)**) and with the false ceiling (**Fig. 33(b)**).

At this position (x = 2 m), a similar flow uniformity can be seen to that at x = 1 m (**Fig. 32**). The ratio between the standard deviation (σ) and average velocities in the regions -0.5 m ≤ y ≤ 0.5 m and -0.5m ≤ z ≤0.5 m is 0.01.

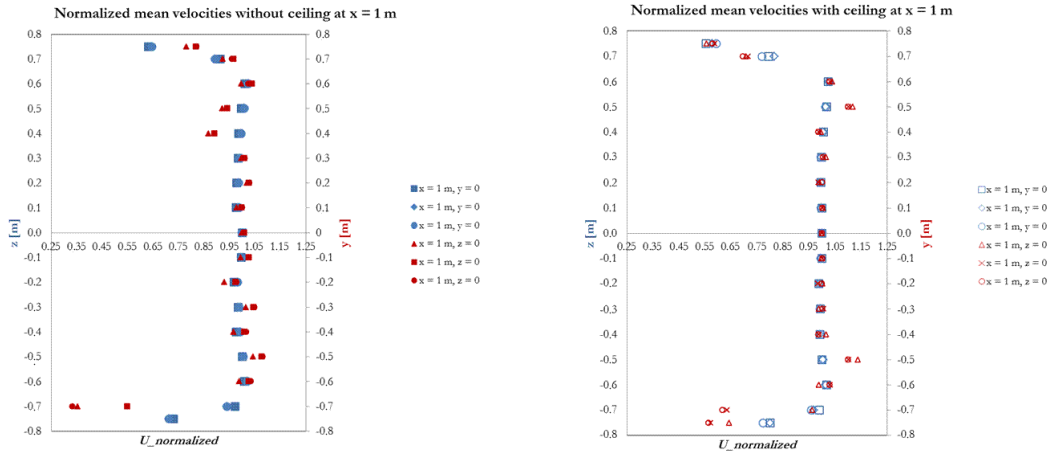

Figure 32: Normalized average flow velocity profiles along the z-vertical and y-horizontal directions at x = 1m from the nozzle exit. (a) Profiles without a false ceiling and (b) profiles with a false ceiling.

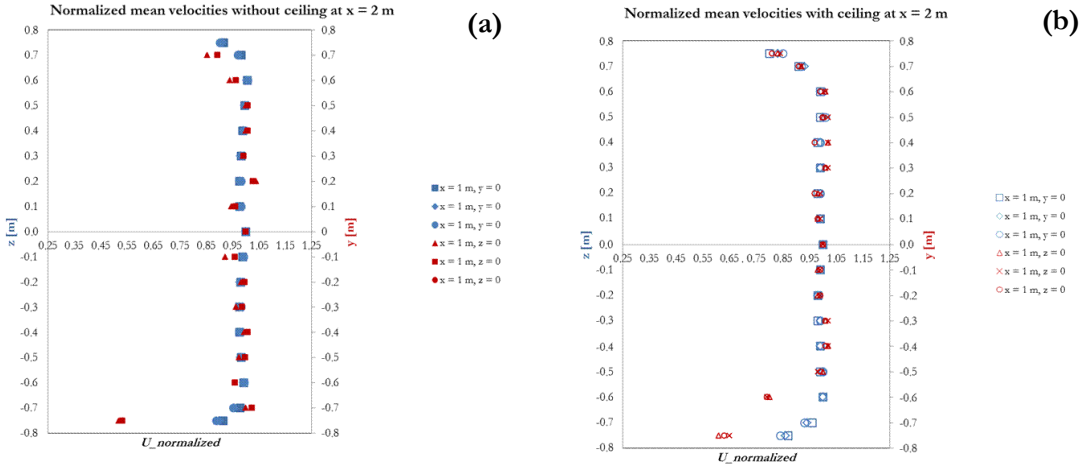

Figure 33: Normalized average flow velocity profiles along the z-vertical and y-horizontal directions at x = 2m from the nozzle exit. (a) Profiles without a false ceiling and (b) profiles with a false ceiling.

Figure 34 shows velocity profiles along the vertical z-direction and along the horizontal y-direction at x = 1 m without the false ceiling and with the false ceiling. The comparison of the velocities at the axis of the exit (i.e., y = 0 and z = 0) indicates a velocity increment of about 0.5 m/s with the ceiling.

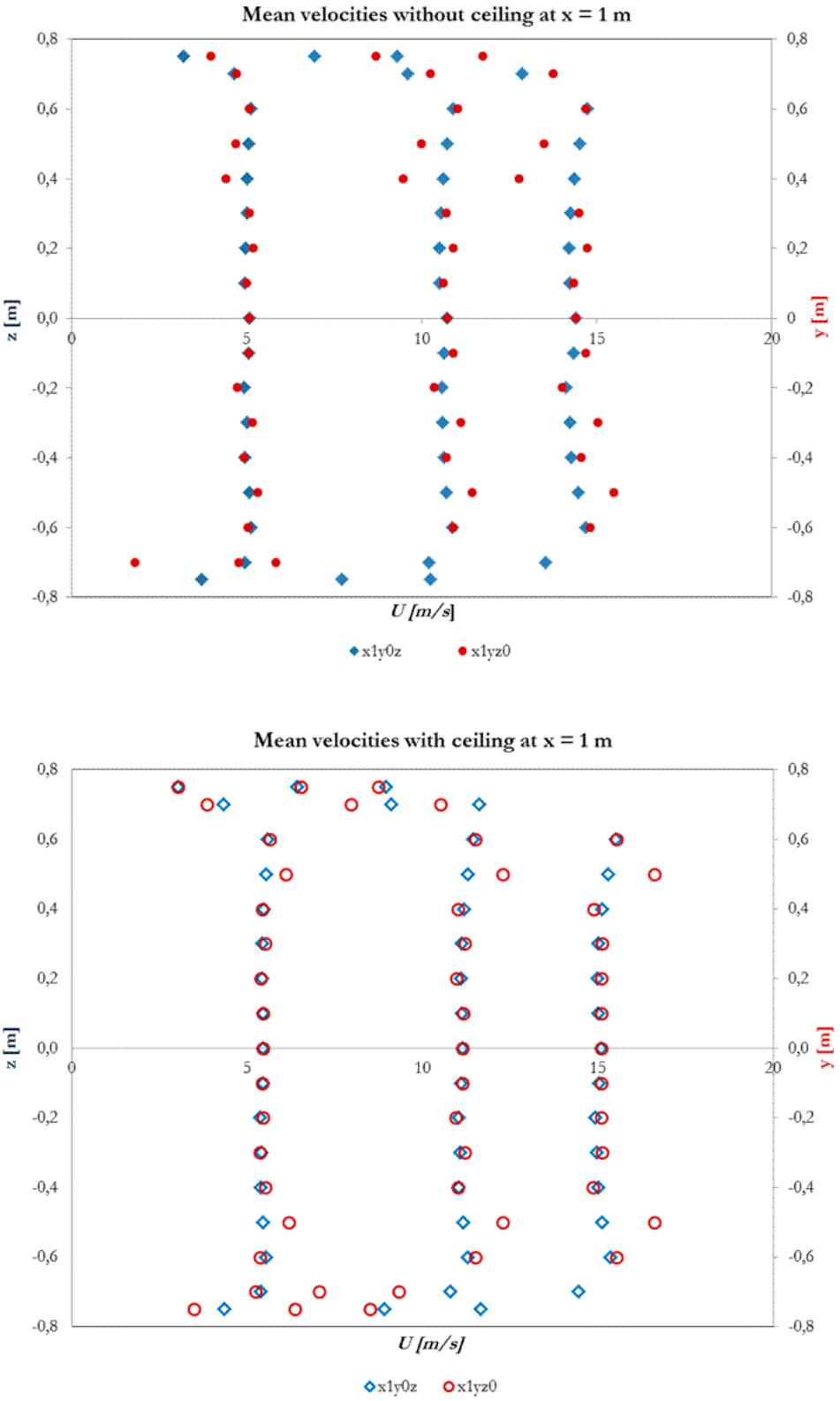

Figure 34: Velocity profiles along the vertical z-direction and along the horizontal y-direction at x = 1 m without the false ceiling and with the false ceiling.

Figure 35 represents a surface plot by Matlab of the mean velocities. The figure has been obtained with the measured points along positive y-axis and positive and negative z-axis in a plane of the test section. This figure illustrates mean velocity plane of a part of the test section, i.e. the flow distribution along positive y-axis and along positive and negative z-axis at x=1m with false ceiling.

A 3D plot with the flow distribution in part of the test section shows a uniform flow uniformity in x = 1 m, $0 \leq y \leq 0.4$ m and -0.4 m $\leq z \leq 0.4$ m.

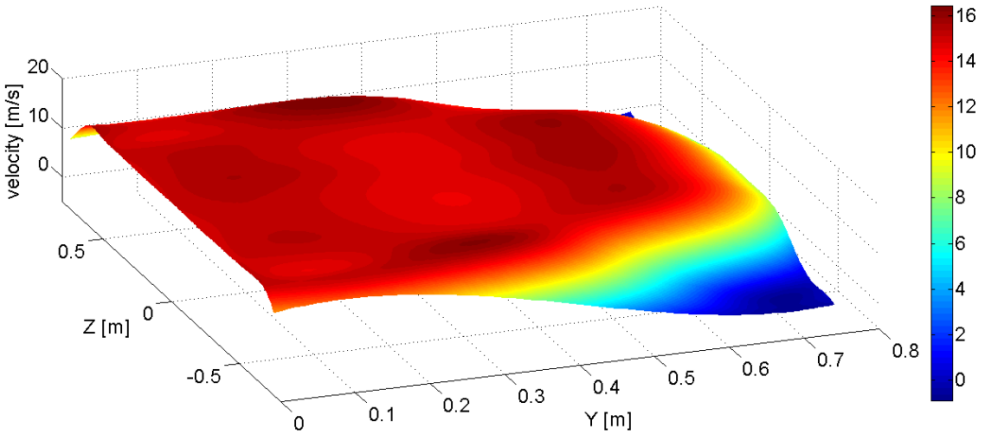

Figure 35: The 3D graph presents mean velocity along positive y-axis and z-axis at x = 1 m.

5.1.3 Turbulence intensities

The profiles of the turbulence intensities are shown and **Figure 36** at (x=1m) and **Figure 37** at (x=2 m). The turbulence intensity (*Ti*) has been calculated considering the root mean square (RMS) of the signal of the single hot wire, which was oriented perpendicular to the flow during the experiments. As shown in **Figure 34** the profiles are plotted along the y and z directions at three different velocities. It can be seen that at x =1 m the false ceiling produces a more uniform distribution of the intensity of the velocity fluctuation and an overall reduction of the turbulence intensity of about 3% with respect to the case without the false ceiling. The measured velocity and turbulence intensity profiles indicate that the flow has a relatively constant velocity and maximum turbulence intensities of 4% in a region with a cross sectional area of 0.8 x 0.8 m^2 and a streamwise dimension of 2 m from the exit of the tunnel.

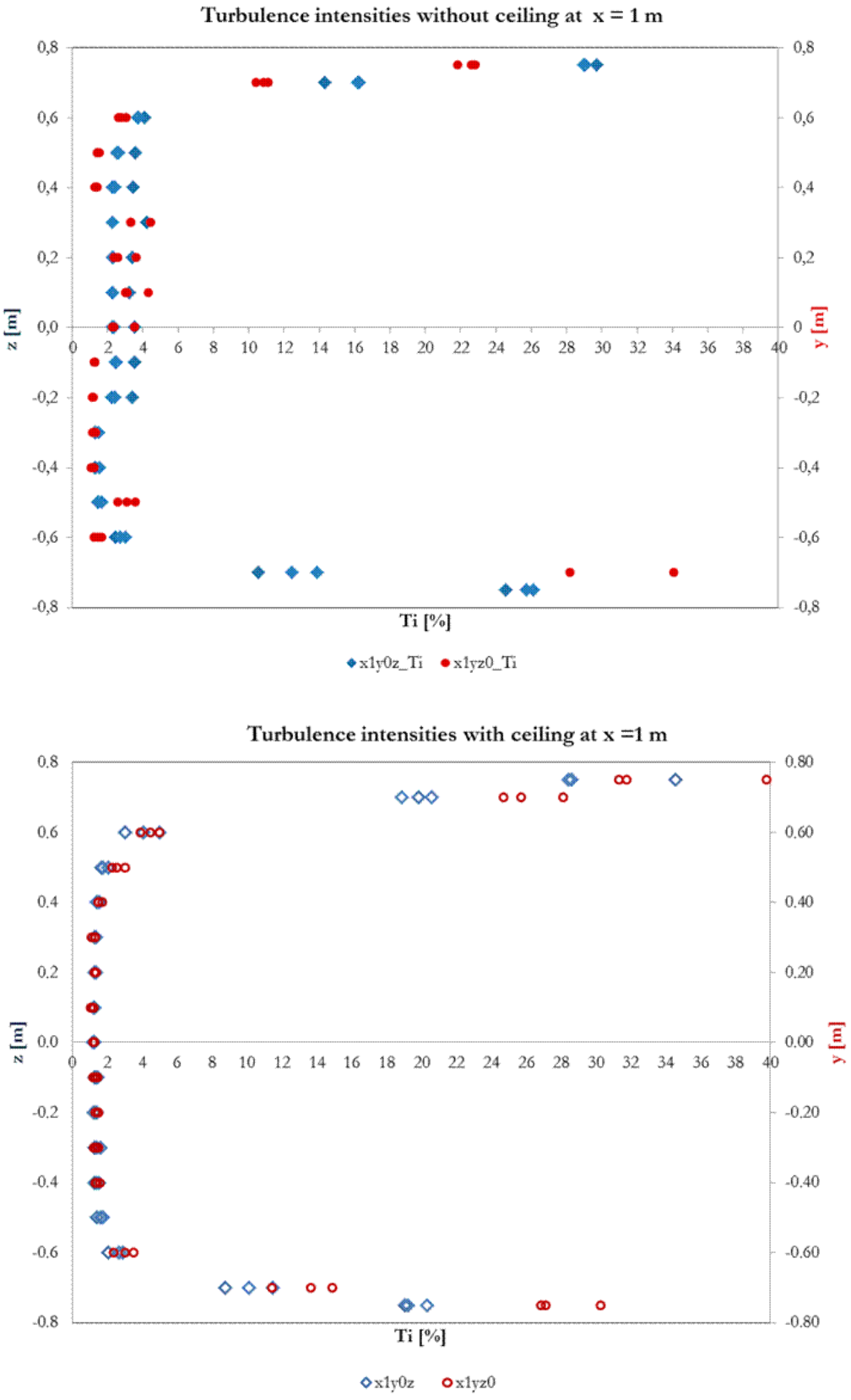

Figure 36: The profiles of the turbulence intensities with and without false ceiling at x = 1m.

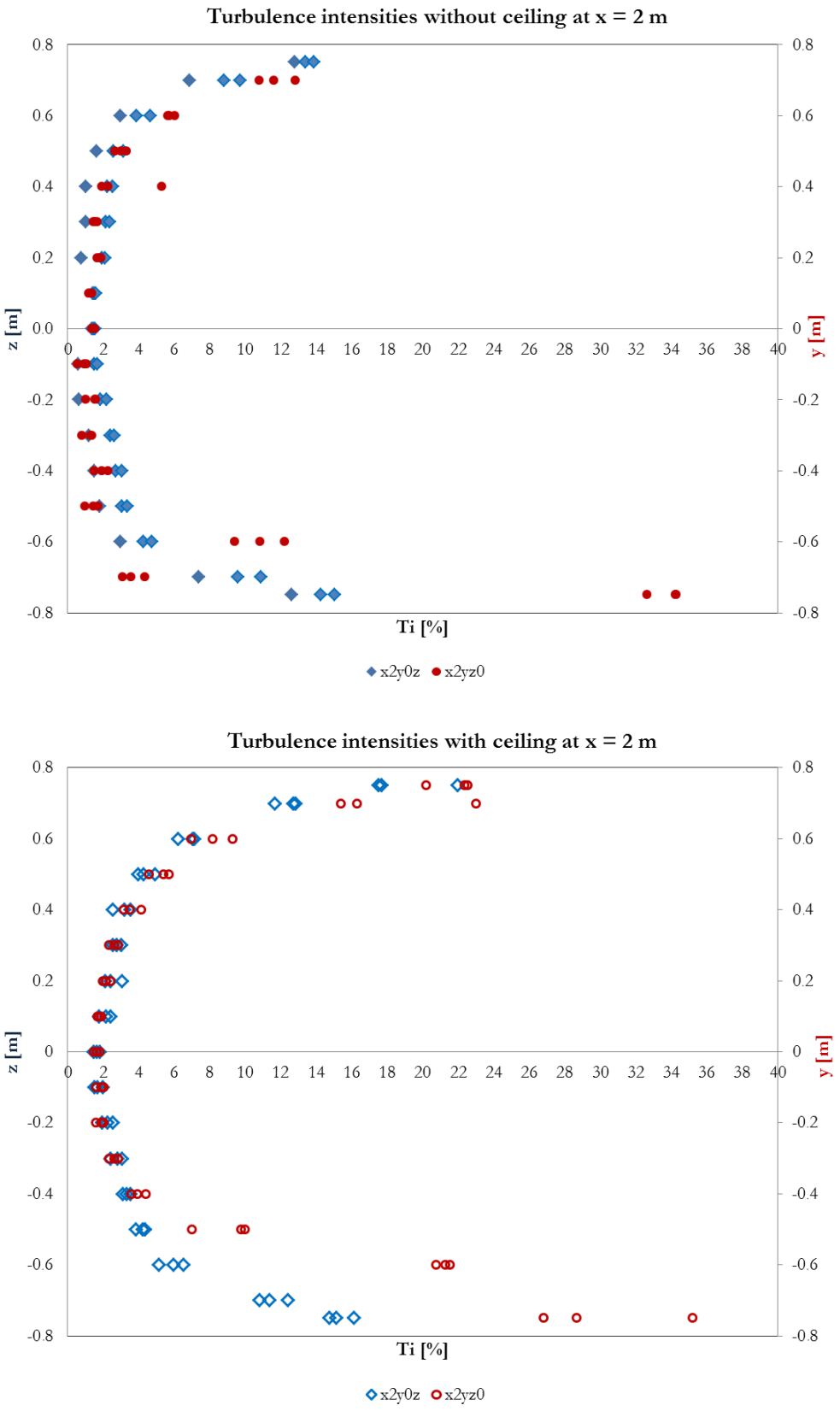

Figure 37: The profiles of the turbulence intensities without and with false ceiling at x = 2 m.

5.1.4 Power spectra

Records of the flow at the locations x=0, y=0, z=0 and x =1 m, y = 0 and z = 0 were obtained with the hot-wire probe to analyse the spectral characteristics of the velocity signal for different velocities at the exit of the tunnel. Two time series at two different wind speeds with 60 seconds and 300 seconds duration were conditioned without low-pass filter and sampled at 10 and 30 kHz, respectively (See Table 3).

location	$U\ [m/s]$	$f_{acq}\ [kHz]$	$t_s\ [s]$
x = 1 m, y = 0, z = 0	4.4	10	60
x = 0, y = 0, z = 0	5.4	30	300
x = 1 m, y = 0, z = 0	12.1	10	60
x = 0, y = 0, z = 0	14.9	30	300

Table 3: Measurement characteristics for spectral analysis.

The spectral analysis was assisted by Dr. Søren Larsen of DTU Wind Energy at Campus Risø in Roskilde, Denmark. This analysis was conducted following Welch's method [34], using partitions of 800000 samples for the long and 60000 for the short time series, respectively. Furthermore, the time series are low-pass filtered with a limit frequency of 500 Hz and after subtraction of the mean value *U*, the mean deviation hereafter is normalized with the standard deviation. Hereby the variance of the normalized time series is equal to 1. The power spectra are shown in Figure 5, together with the Davenport spectrum [35], Equation (19). Davenport spectrum is considered as a good mathematical representation for the horizontal wind fluctuations:

$$psd \quad \frac{2/3\left(f\frac{Lu}{U}\right)^2}{\left(1+\left(f\frac{Lu}{U}\right)^2\right)^{4/3}} \qquad (19)$$

Figure 38 the Davenport spectrum is fitted with a length scale *"Lu"* equal to 0.1 m. The plot shows that, following Taylor's hypothesis of frozen turbulence [36] and [37], the standard deviation of the wind speed scales well with the averaged velocity. Additionally,

the figure illustrates that the spectra increase at high frequencies, reflecting signal noise, which we have only partially removed by the low-pass filtering. However, with the Taylor's frozen turbulence assumption applied, the plots of the normalized spectra indicate that the spectra follow "normal atmospheric boundary layer (ABL) turbulence" behaviour with a production range around f/U ≈ 10 followed by an inertial subrange shown by a -2/3 slope turbulence. At high frequencies the dissipation region is partly shown but part is hidden by the high frequency noise. As demonstrated with the curve showing the Davenport spectrum, this spectral form reproduces quite well the tunnel spectrum, provided that the production scale of the Davenport spectrum (1200 m) is replaced by the scale for the production scale for the tunnel turbulence (L_u = 0.1 m), reflecting vortices being created by means of propellers. This can be seen as an indication that the wind tunnel is suitable to study wind effects on a scaled wind turbine in a comparable way as with a real turbine operating in the ABL.

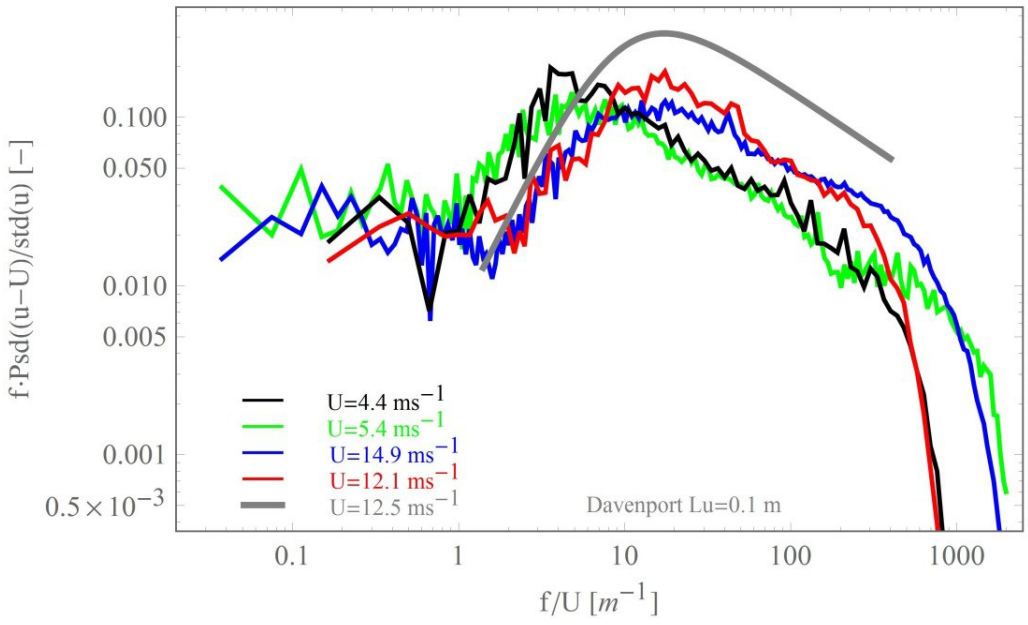

Figure 38: Comparison of dimensionless spectra of the flow at the central axis of the wind tunnel.

5.2 Cup anemometer calibration results

5.2.1 Blockage effect of the cup anemometer on pitot tubes

In order to verify the influence between the cup anemometer and pitot tubes this test was carried out. The measurement instruments used were:

a- Cup Anemometer calibrated in WindTunnel of Deutsche Wind Guard, Varel.
b- NPL 8 mm pitot tubes calibrated below laboratory accreditation requirements of the United Kingdom Accreditation Service (UKAS).
c- Setra C 239 differential pressure transducers calibrated by NIST RPT 1500129433.

The working grid of this test is presented in the next figure where blue points are the pitot tubes, the arrows indicate the direction of movement of the pitots, orange lines delimit the uniform test section. **Figure 39** shows the initial position of the cup anemometer and pitot tubes. Cup anemometer was positioned at x = 1.5 m, y = 0 and z = 0. Pitot tube 1 (P1) was positioned at x =1.5 m, y = -0.4 m and z = 0 m, Pitot tube 2 (P2) at x = 1.5 m, y = 0 and z = 0.4 m, Pitot tube 3 (P3) at x = 1.5 m, y = 0.4 m and z = 0. Finally pitot tube 4 (P4ref) was positioned at x = 1.5 m, y = -0.4 m and z = 0.4 m and it was the reference point.

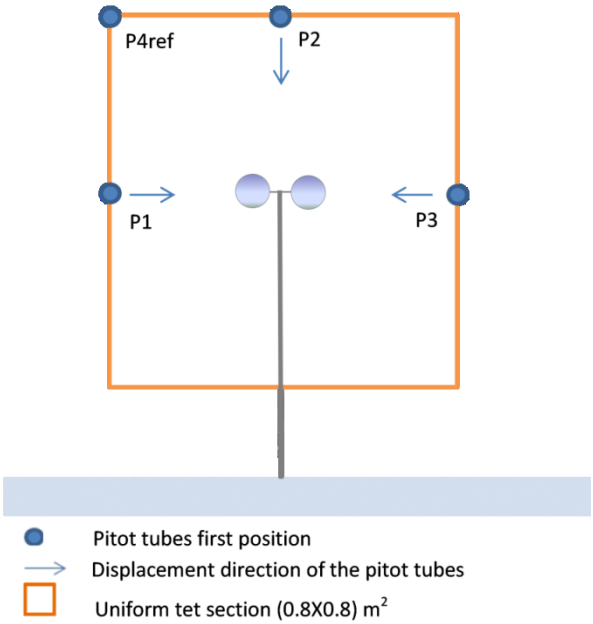

Figure 39: Initial position of cup anemometer and pitot tubes. Cup anemometer initial position (1.5;0;0)m. P3 (1.5;0.4;0) m, P1 (1.5;-0.4;0) m, P2(1.5;0;0.4) m and P4ref (1.5;-0.4;0.4) m.

Running the wind tunnel and displacing P1, P2 and P3 and conserving P4ref and the cup anemometer in the same position, the results obtained are shown in **.** The y-axis presents the distances of the pitot tubes from the cup anemometer. All velocities measured have been normalized to the mean speed obtained in the initial measures and positions show in the plot of the working grid. The results present less influence between pitot tubes and cup anemometer from 30 cm of distances each other.

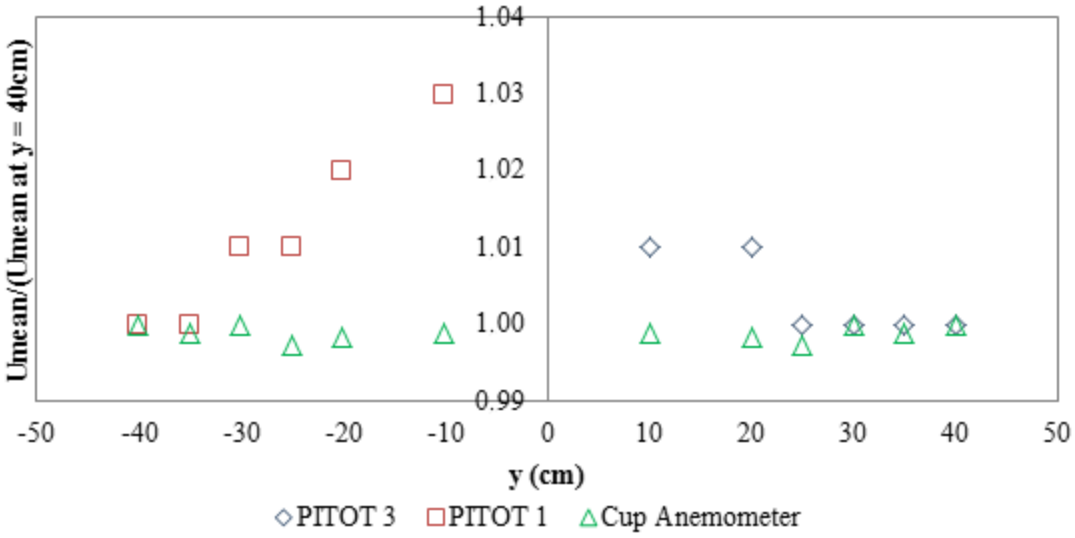

Figure 40: Mean speeds normalized to mean speeds obtained in the initial measures and positions of measurement instruments.

5.2.2 Cup anemometer calibration

Figure 41 shows the averaged measured velocity with the four pitot tubes with the cup anemometer located in the centre as illustrated in **Figure 29**. The flow velocities measured with the cup anemometer and the averaged measured velocities with the four pitot tubes without the cup anemometer are also included. The first figure corresponds to measurements performed without the false ceiling and the second to measurements with the false ceiling. The comparison between both figures shows that a better flow distribution is obtained with the false ceiling (i.e. the three values of the flow velocity are more coincident).

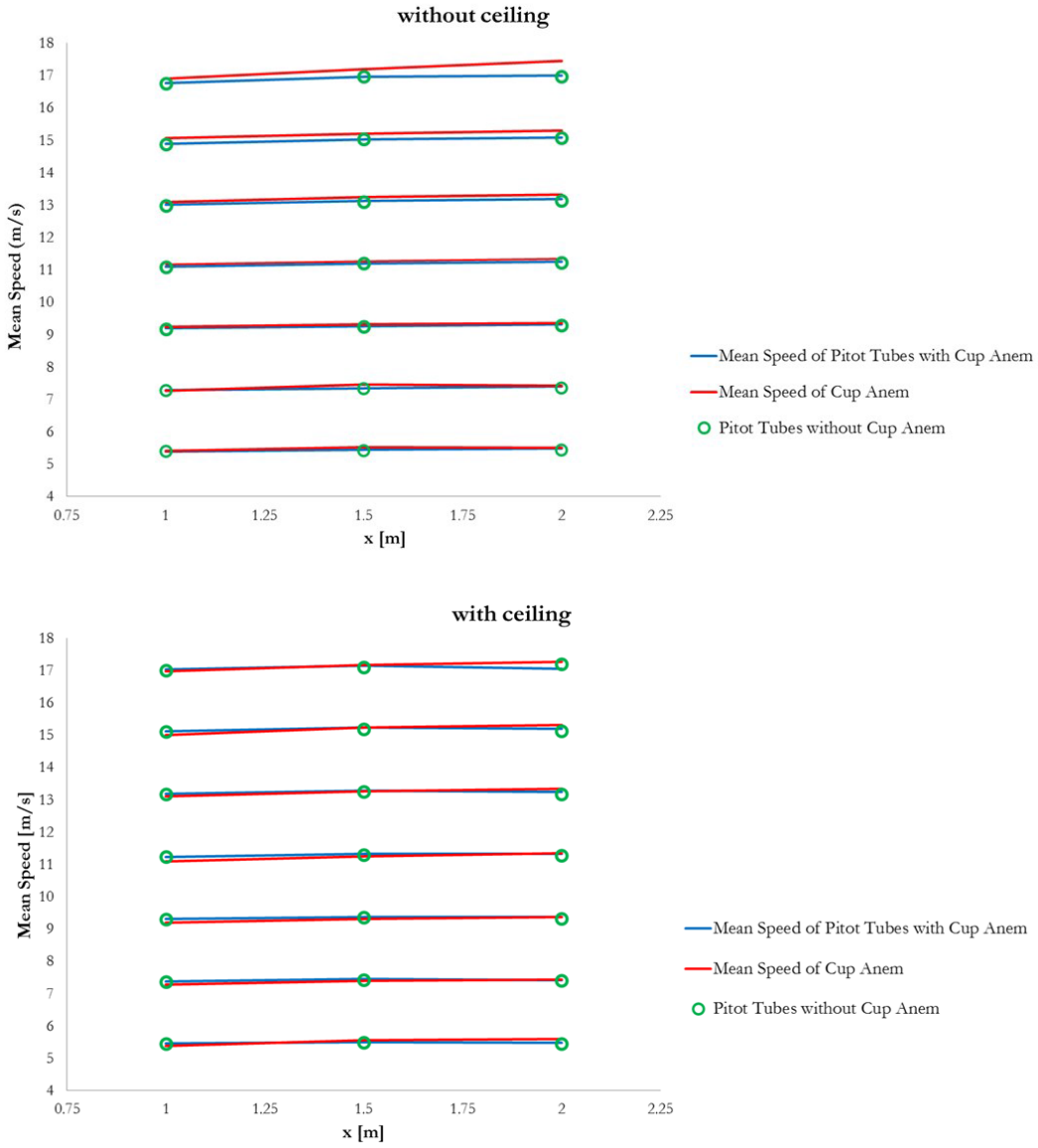

Figure 41: Mean velocities without and with false ceiling at different positions from de nozzle (x-axis). Blue lines, average velocities with 4 pitot tubes + Cup anemometer. Red lines mean velocities with cup anemometer only positioned in the centre of the test area. Green circles average velocities with four pitot tubes only.

Finally the calibration results of the cup anemometer with the false ceiling are explained. The test conditions were: wind tunnel exit area = 2.25 m^2; anemometer frontal area = 0.022m^2, diameter of the mounting bar = 28 mm, blockage ratio 0.01, temperature 25.09 ± 0.1ºC, atmospheric pressure 1005 hPa ± 1.3 hPa and relative air humidity equal 38 % ± 1%.

The linear fit of the anemometer response in each position indicated by red circles in **Figure 28** are shown in the next figures.

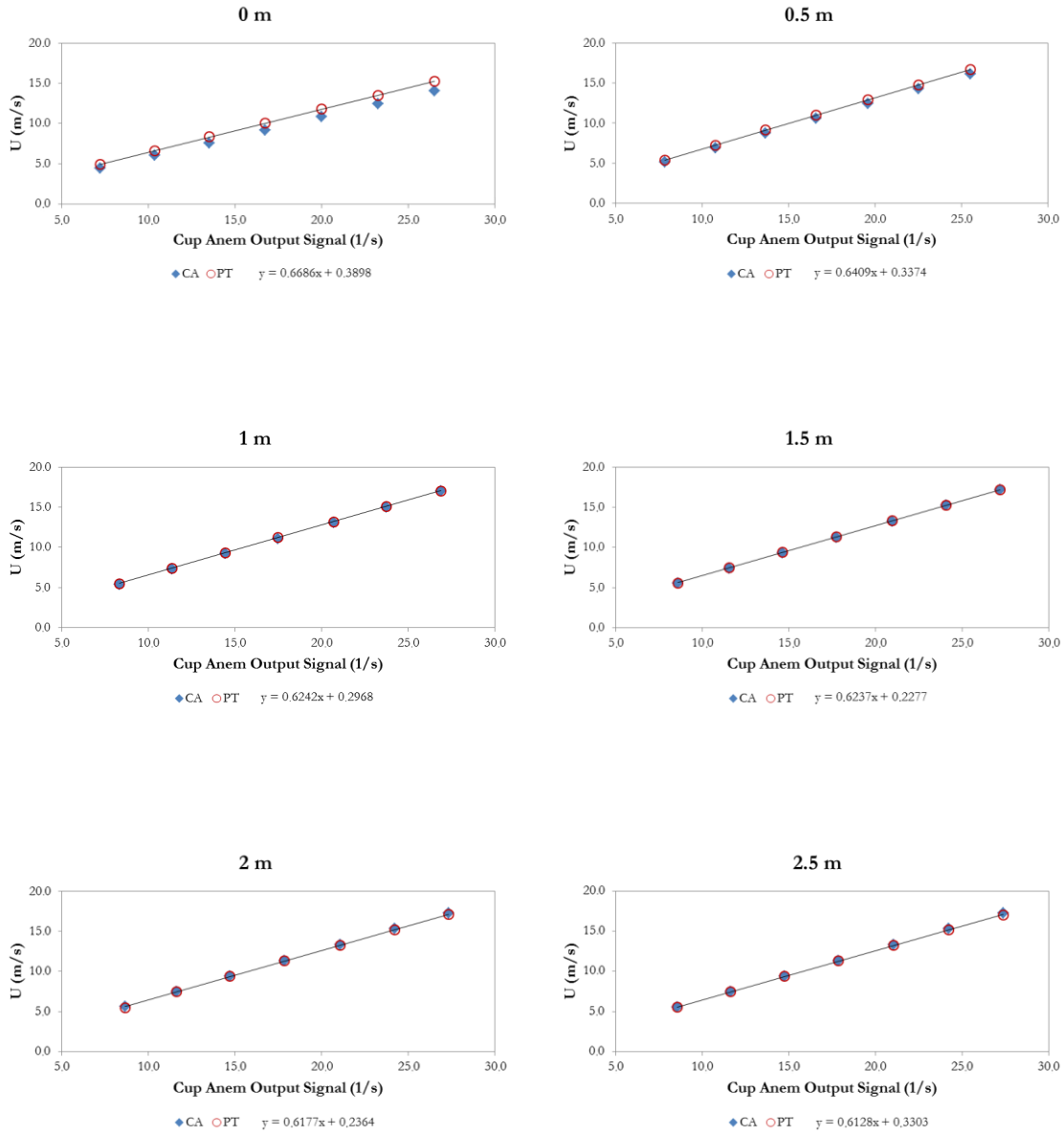

Figure 42: Average speeds by cup anemometer (CA). Average speeds by pitot tubes (PT). Linear fit obtained.

Based in the standard deviation between the average speed given by the cup anemometer and the average speed given by 4 pitots, the best linear fit of the anemometer response was

found when the cup anemometer was positioned at x = 1 m from the nozzle exit. The line fit obtained was *y=0.6242x+0.2968* (Figure 43).

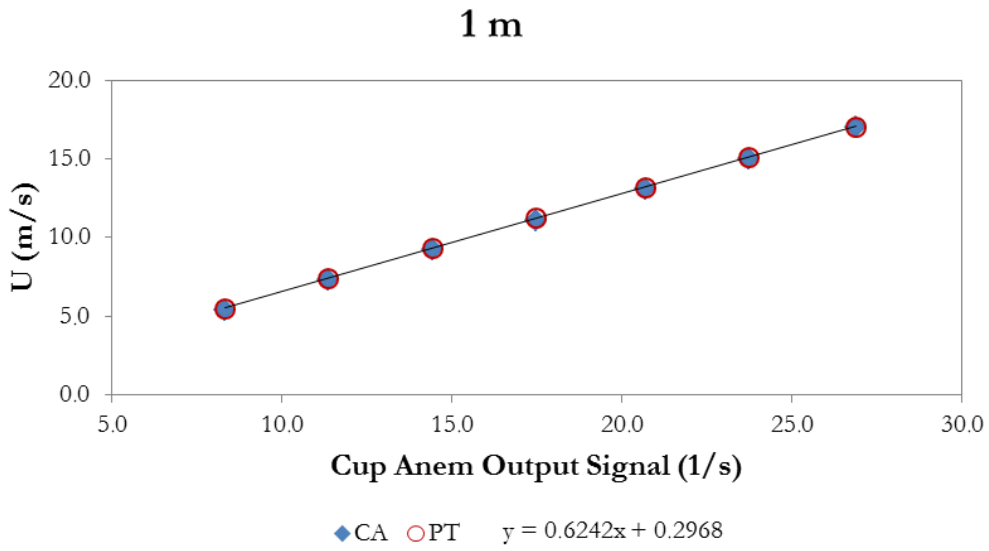

Figure 43: Average speeds by cup anemometer (CA). Average speeds by pitot tubes (PT). Linear fit obtained in 4-Winds OJWT *[Slope=0.6242(m/s)/(1/s). Offset=0.297(m/s)].*

Table 4 shows the cup anemometer output signal (1/s), the average speeds based on the linear fit of the certificate calibration *[Slope=0.6245(m/s)/(1/s). Offset=0.194(m/s)],* the tunnel speed averaged between the 4 pitot tubes located at the corners of the uniform test section and relative errors between the averaged speeds measured with the pitot tubes and average speeds measured with the calibrated cup anemometer, it can be seen that the relative errors are less than 1.5 %.

Cup Anemometer output Signal (1/s)	Tunnel Speed based on the line fit of the accredited certificate (m/s)	Average Tunnel Speed of 4 pitot tubes (m/s)	Err %
8.33	5.39	5.46	1.29
11.34	7.28	7.38	1.43
14.42	9.20	9.31	1.17
17.45	11.09	11.23	1.26
20.67	13.10	13.19	0.63
23.72	15.00	15.12	0.75
23.78	16.97	17.03	0.37
23.78	15.04	15.10	0.39
20.59	13.05	13.17	0.93
17.47	11.10	11.23	1.15
14.39	9.18	9.29	1.21
11.37	7.30	7.37	0.97
8.30	5.38	5.45	1.49

Table 4: Cup anemometer output signal (1/s); Average speeds based on linear fit of the certificate calibration *[Slope= 0.6245 (m/s) / (1/s). Offset = 0.194(m/s)]*; Average tunnel speed between 4 pitot tubes positioned in every corner of the uniform test section and relative errors between average speeds of pitot tubes and average speeds measured with the calibrated cup anemometer.

Chapter 6

CONCLUSIONS AND FUTURE WORK

Design criteria and layout options for an open jet wind tunnel have been discussed and the performance characteristics of the facility have been shown in detail. The final design of the open jet tunnel is original and it allows a good performance at a relatively low cost.

The wind tunnel is driven by four axial fans of 7.5 kW each, with a diameter of 1 m and placed in a 2.24 m x 2.24 m matrix. They operate at a maximum speed of 1440 rpm and they are controlled by a variable frequency electronic device. Airflow enters the wind tunnel through a plenum chamber with a safety screen at the end. Then a honeycomb and two screens for the purposes of flow straightening and turbulence reduction have been disposed. Finally, the open jet exits into the test section from the contraction nozzle. The contraction with a ratio of 2.23 and a length of 1 m increases the flow speed. The shape of the nozzle is not conventional but flow shows appropriate characteristics in a central section of the jet with a cross section of 0.8 m x 0.8 m and distances from the jet exit from 1 m to 2 m. The estimated maximum velocity attainable in the test section is 17 m/s; thus the maximum Reynolds number calculated based on the hydraulic diameter of the test section is 1.96×10^6. The flow is expanded freely into the laboratory where it was placed. A security cage is used as the instrument carriage as well as the safety system for researchers and technicians of the tunnel.

The facility was characterized to ensure the quality of the aerodynamic and acoustic measurements. The characterization experiments were performed up to a test section speed of $U = 17$ m/s. The characteristics of the tunnel show that it can be operated at constant average velocities and relatively low turbulence intensities. The analysis of the velocity signal, measured with a hot wire probe, indicates that the measured power spectrum has similar characteristics than that of the atmospheric turbulence.

Simultaneous flow measurements with a calibrated cup anemometer and with pitot tubes distributed within the test section show that the tunnel can be used to test small scale wind turbines and for calibration purposes.

The above results have been carried out during 2013. A new characterization should be considered. Static pressure measurements along the sidewall, base, and corners of the contraction to validate the design procedure to generate a minimum-length contraction devoid of flow separation, as well as shear layer measurements in order to quantify the growth of the test section jet should be included as additional characterization.

A Future numerical research, with the final characteristics of the 4-Winds OJWT, should be continued to complete the characterization of the facility. A comparison between numerical and experimental results proves an interesting challenge.

References

[1] S. Mertens, "Wind energy in urban areas: Concentrator effects for wind turbines close to buildings," pp. 22-24, 2002.

[2] Ministerio de industria, "La energía en España," Madrid, Centro de publicaciones del gobierno, 2013.

[3] "Catalogue of Small Wind Turbines," Preben Maegaard, Anna Krenz & Wolfgang Palz, 2014.

[4] M. C. Remillieux, E. D. Crede, H. E. Camargo, R. A. Burdisso, W. J. Devenport., M. Rasnick, P. Van Seeters and A. Chou, "Calibration and demonstration of the new Virginia Tech anechoic wind tunnel," *American Institute of Aeronautics and Astronautics,* 2008.

[5] J. Mathew, C. Bahr , B. Carroll, M. Sheplak and L. Cattafesta, "Design, fabrication, and characterization of an anechoic wind tunnel facility," in *11th AIAA/CEAS Aeroacoustics Conference*, Monterey, CA, 2005.

[6] H. H. Hubbard and J. C. Manning, "Aeroacoustic research facilities at NASA Langley Research Center, description and operational characteristics.," NASA Technical Memorandum 84585, Hampton, Virginia, 1983.nb

[7] T. Chong , P. Joseph and P. Davies , "Design and performance of an open jet wind tunnel for aero-acoustic measurement," *Appl Acoust,* p. 70:605–14., 2009.

[8] C. E. Hanson, "The design, development and construction of a low noise, low-turbulence wind tunnel," Massachusetts. EEUU, 1967.

[9] J. Winkler, F. Temel and T. Carolus, "Concept, design and characterization of a small aeroacoustic wind tunnel facility with application to fan blade measurements," in *Fan Noise*, Lyon, France, 2007.

[10] A. Sedaghat , . X. Liu, J. Whitty and . X. Tang, "Wind power of small wind turbines in turbulent open jets," *Scientia Iranica,* vol. 19, no. 2, pp. 272-281, 2012.

[11] D. Sims-Williams and R. Dominy, "The Design of an Open-Jet Wind Tunnel for Model Testing," in *Motorsports Engineering Conference & Exhibition*, 2002.

[12] L. Lignarolo, D. Ragni, C. Krishnaswami, Q. Chen, C. Simão Ferreira and G. van Bussel, "Experimental analysis of the wake of a horizontal-axis wind-turbine," *Renewable Energy,* vol. 70, no. (2014), pp. 31-46, 2014.

[13] J. Yen and N. Ahmed, "Improving safety and performance of small-scale vertical axis wind turbines," *SciVerse ScienceDirect, Procedia Engineering,* vol. 49, pp. 99-106, 2012.

[14] S. Mertens, Wind Energy in the Built Environment, Concentrator Effects of Buildings, Essex, United Kingdom: Multi-Science, 2006.

[15] H. Riazi and N. Ahmed, "Numerical Investigation on Two-Orifice Synthetic Jet Actuators of Varying Orifice Spacing and Diameter," *29th AIAA Applied Aerodynamics Conference,* no. 3171, 2011.

[16] N. Findanis and N. Ahmed, "Three-Dimensional Flow Reversal and Wake Characterisation of a Sphere Modified with Active Flow Control Using Synthetic Jet," in *Advances and Applications in Fluid Mechanics*, 2011.

[17] S. Pindado, J. Cubas and Á. Sanz-And, "Aerodynamic Analysis of Cup Anemometers Performance:," vol. 2013.

[18] J. Meseguer, A. Sanz-Andrés, S. Franchini and S. Pindado, "Instalaciones de Aerodinámica Experimental para Ingeniería Civil de la Universidad Politécnica de Madrid," 2007.

[19] N. Ahmed and N. Findanis, "Wind Tunnel "Concept of Proof" Investigations in the Development of Novel Fluid Mechanical Methodologies and Devices, Wind Tunnel and Exprimental Fluid DynamicsResearch," p. 135, 2011.

[20] J. Meseguer Ruiz and A. Sanz Andrés, Aerodinámica Básica, Madrid: Garceta, 2005.

[21] A. Pope and W. Rae, Low-speed wind tunnel testing, John Wiley and Sons, 1984.

[22] R. Mehta and P. Bradshaw, "Design rules for small low speed wind tunnels," *The Aeronautical Journal of the Royal Aeronautical Society,* pp. 443-449, 1979.

[23] A. Pope and J. J. Harper, Low Speed Wind Tunnel Testing, Wiley, 1966.

[24] J. Scheiman and J. Brooks, "Comparison of Experimental and Theoretical Turbulence Reduction Screens, Honeycomb, and Honeycomb-Screen Combination.," *J.Aircraft,* vol. (8), no. 18, pp. 638-643, 1981.

[25] R. Loehrke and H. Nagib, "Experiments on Management of Free-Stream Turbulence," 1972.

[26] H. Roberts, "Consideration in the Design of a Low-Cost Wind Tunnel," in *Fourteenth Annual Meeting of the Institute of Aeronautical Sciences*, 1946.

[27] I. Idel'chik, "Handbook of Hydraulic Resistance," no. AEC-TR-6630, 1966.

[28] W. Eckert, K. Mort and J. Jope, "Aerodynamic Design Guidelines and Computer Program for Estimation of Subsonic Wind Tunnel Performance," 1976.

[29] G. I. Derbunivich, A. S. Zemskaya and E. U. Repik, Effect of Flow Contraction on the Level of Turbulence, vol. 2, Izvestiya Akademii Nauk SSSr, 1987, pp. 146-152.

[30] I. ANSYS, "ANSYS Fluent Tutorial Guide," ANSYS, Inc., 2013.

[31] N. Rajaratnam, "Turbulent Jets," *Elsevier Scientific Publishing Company,* 1976.

[32] E. Jørgensen Finn, "How to measure turbulence with hot-wire anemometers a practical guide," Dantec Dynamics, Skovlunde, Denmark, 2002.

[33] O. University, "DRAFT DEWI 1095 Anemometer Calibration at the Wind Tunnel.," 2011.

[34] P. D. Welch, "The use of Fast Fourier Transform for the estimation of the power spectra: A method based on time averaging over short, modified periodograms," Vols. AU-15, pp. 70-73, 1967.

[35] A. G. Davenport, "The spectrum of horizontal gustiness near the ground in high winds," vol. 87, p. 194–211, 1961.

[36] G. I. Taylor, "The Spectrum of Turbulence," in *Proceedings of the Royal Society of London. Series A, Mathematical and Physical Sciences*, London, 1938.

[37] N. Isyumov , "Alan G. Davenport's mark on wind engineering," 2012.

[38] M. Kim, J. Lee, J. Kee and J. Chang, "Hyundai Full Scale Aero-acoustic Wind Tunnel," *SAE Technical Paper 2001-01-0629,* 2001.

[39] C. W. E. Association, "Small Wind Turbine Purchasing Guide," 2016.

UNIVERSITAT ROVIRA I VIRGILI
ESTUDI NUMÈRIC I EXPERIMENTAL DEL SOROLL AERODINÀMIC GENERAT PER UNA TURBINA PETITA D'EIX VERTICAL
Silvana Cecilia Tourn Cremona

Este ejemplar
se terminó de imprimir
en noviembre de 2017, en

Tel. +54 362 4572483
vianetchaco@yahoo.com.ar
Av. Las Heras 526 Dto. B
Resistencia, Chaco
República Argentina.

UNIVERSITAT ROVIRA I VIRGILI
ESTUDI NUMÈRIC I EXPERIMENTAL DEL SOROLL AERODINÀMIC GENERAT PER UNA TURBINA PETITA D'EIX VERTICAL
Silvana Cecilia Tourn Cremona

UNIVERSITAT ROVIRA I VIRGILI
ESTUDI NUMÈRIC I EXPERIMENTAL DEL SOROLL AERODINÀMIC GENERAT PER UNA TURBINA PETITA D'EIX VERTICAL
Silvana Cecilia Tourn Cremona

UNIVERSITAT
ROVIRA i VIRGILI